TITLE

Mediator 1 ablation induces enamel-to-hair lineage conversion through enhancer dynamics

AUTHOR LIST

Roman Thaler[1], Keigo Yoshizaki[2], Thai Nguyen[6], Satoshi Fukumoto[3,4], Pamela Den Besten[5], Daniel D. Bikle[6], Yuko Oda[6]*

AFFILIATIONS

[1] Department of Orthopedic Surgery, Mayo Clinic, Rochester, MN, USA
[2] Section of Orthodontics and Dentofacial Orthopedics, Division of Oral Health, Growth and Development, Kyushu University Faculty of Dental Science, Fukuoka, Japan.
[3] Section of Pediatric Dentistry, Division of Oral Health, Growth and Development, Kyushu University Faculty of Dental Science, Fukuoka, Japan
[4] Division of Pediatric Dentistry, Department of Oral Health and Development Sciences, Tohoku University Graduate School of Dentistry, Sendai, Japan
[5] Department of Dentistry, University of California San Francisco, CA, USA
[6]Departments of Medicine and Endocrinology, University of California San Francisco and Veterans Affairs Health Center San Francisco, CA, USA

ORCID number YO: 0000-0001-6124-3530

* Correspondence to: yuko.oda@ucsf.edu (YO)

Short title: *Med1* controls ectodermal lineage

ABSTRACT

Adult stem cell fate has been postulated to be primarily determined by the local tissue microenvironment. Here, we found that Mediator 1 (Med1) dependent epigenetic mechanisms dictate tissue-specific lineage commitment and progression of dental epithelial stem cells. Conditional loss of *Med1*, a key component of the Mediator complex linking enhancer activities to gene transcription, provokes a tissue extrinsic lineage shift, causing hair generation in the dental environment. Mechanistically, we found that Med1 establishes super-enhancers that control enamel lineage driven transcription factors in control dental stem cells and progenies. However, *Med1* deficiency ablates this epigenetic circuit and causes a switch from the dental epithelial transcriptional program towards hair and epidermis on incisors *in vivo,* and in dental stem cell culture *in vitro*. *Med1* loss also provokes an increase in enhancers and super-enhancers near epidermal and hair genes. Interestingly, control incisors already exhibit enhancers near hair and epidermal key transcription factors; these expand in size and transform into super-enhancers upon *Med1* loss indicating that these epigenetic mechanisms cause the transcriptomic and phenotypic shift towards epidermal and hair lineages. Thus, we propose a role for Med1 as safeguard of the tissue-specific epigenome during adult stem cell differentiation, highlight the central role of enhancer accessibility and usage in adult stem cell lineage and provide new insights into ectodermal regeneration.

INTRODUCTION

Postnatal cell fate determination of multipotent adult stem cells is controlled by selective transcriptional programs, that are coordinated by an underlying epigenetic machinery and tissue intrinsic microenvironments[1-4]. Ectoderm derived epithelial stem cells can evolve into multiple lineages and depending on their homing tissue, stem cells differentiate into enamel forming dental lineages, or to hair and epidermis generating skin epithelia[5-7]. Intriguingly, adult stem cells often retain an inclination to their tissue of origin *in vitro* as well as their differentiation potential often reflects their provenance in culture[3,8,9]. Thus, although multipotent adult stem cells have the potential to differentiate into different cell clades, they are endowed with tissue-specific potency[8]. To date, the mechanisms controlling tissue-specific stem cell differentiation are yet not fully understood, and accordingly, the factors safeguarding tissue selective dental or epidermal cell fate determination are still largely elusive. Understanding these mechanisms is also crucial for our efforts in combating diseases like alopecia, ectodermal dysplasia or tooth loss as it might create new entry points for the development of bioengineering strategies for the regeneration of tissues like tooth enamel and skin hair, which has been challenging[7].

The mouse incisor provides an excellent model system to study adult stem cell fate. Dental epithelial stem cells (DE-SCs) residing in the cervical loop (CL) at the proximal end of incisors support the continuous growth of the incisors throughout the lifespan of a mouse. They regenerate the enamel organ by giving rise to all the dental epithelia such as enamel matrix producing ameloblasts, Notch1 regulated stratum intermedium (SI) and others[10-15].

70 Skin epithelia derived from the same ectoderm are divided into the interfollicular
71 epidermis and hair follicles during embryonic stages of skin formation[6]. Postnatally, hair
72 follicle stem cells residing in the bulge region of hair follicles regenerate hair in skin[16,17].
73 Hair follicles are essential for hair growth and regeneration in mammalian skin and are
74 characterized by a complex multilayered bulb structure containing the outer and inner root
75 sheath, medulla, and cortex[18,19]. Following the initial developmental cycle, hair is
76 maintained by hair follicle cycling in mice, characterized by an anagen phase during which
77 the hair follicle expands, followed by a transitional catagen phase, leading to the involution
78 of the hair follicle, and telogen, the resting phase. The cycle then begins a new in
79 response to signals from the dermal papilla, a specialized mesenchymal cell attached to
80 the proximal end of the hair bulb[20,21]. The shift between these phases involves substantial
81 changes in gene expression patterns, which can be activated by injury. For example, hair
82 depilation induces new hair growth by stimulating anagen with induction of gene
83 expression such as those encoding hair keratins[22].
84 Several transcription factors (TF) and pathways have been shown to induce dental
85 as well as hair and epidermal cell differentiation. For example, paired like homeodomain
86 2 (*Pitx2)*[23] or *Nkx2-3*[24] *Isl1*[25] are implicated in embryonic enamel epithelial homeostasis[7]
87 while TFs and signaling genes including HR lysine demethylase and nuclear receptor
88 corepressor (*Hr* or *also called hairless*) and Ras and Rab interactor 2 (*Rin2*) are important
89 in controlling hair differentiation because their mutation causes alopecia (hair loss)[26,27].
90 On the other hand, AP1 factors (*Fos/Jun*) and the tumor proteins of the p53 family
91 members including *Tp63* are crucial to direct postnatal epidermal differentiation in the

92 skin[19]. However, the check point factors controlling dental vs epidermal cell fate are still
93 largely elusive.

94 We have shown before that Mediator 1 (Med1) controls dental[28-30], and epidermal
95 cell fates[28,31-34]. Med1 suppression also hinders invariant natural killer T cell
96 development[35] and prevents luminal cell maturation in the mammary epithelia in mice[36,37].
97 These data suggest a role for Med1 in controlling tissue-selective adult stem cell lineage
98 commitment.

99 Med1 is a key subunit of Mediator complex, which facilitates gene transcription by
100 linking enhancers to the RNA polymerase complex at transcriptional start sites (TSS) in
101 gene promoters. Med1 has been shown to localize at typical enhancers (TE) and super-
102 enhancers (SE) which represent distal regulatory elements recognized as key epigenetic
103 hubs to determine cell identity and properties[4,38]. As such, the Mediator complex
104 facilitates the expression of cell fate driving transcription factors and genes in somatic
105 cells[4,38]. Removal of the Med1 subunit abolishes transcription of genes[39], but the exact
106 role of Med1 in the Mediator complex is still not fully understood as studies indicate that
107 Med1 is dispensable for Mediator complex formation[39].

108 In the present study, we investigate the role of Med1 in governing ectoderm lineage
109 determination using a conditional knockout (cKO) mouse model in which *Med1*
110 expression is deleted from ectoderm derived epithelial cells. Med1 ablation provokes a
111 tissue extrinsic lineage shift, causing ectopic hair growth on incisors. Using an integrative
112 multi-omics approach, we demonstrate that this intriguing phenomenon is due to a
113 reshape of the enhancer landscape which causes amplification of ectodermally

114 conserved distal enhancers linked to transcription factors that control epidermal and hair
115 lineage commitment and progression.
116
117 **Results**
118

119 **Lack of *Med1* in dental epithelia causes ectopic hair without morphogenesis of hair**
120 **follicles on incisors.**

121 During postnatal murine tooth maintenance, CL residing dental epithelial stem cells (DE-
122 SCs) differentiate into Notch1 regulated SI, ameloblasts and other epithelia to mineralize
123 enamel on the incisor surface (Fig. 1a, top). Intriguingly, deletion of *Med1* from *Krt14*
124 expressing DE-SCs and progenies provokes a major phenotypical shift in the dental
125 compartment causing enamel formation to be replaced by unusual, ectopic hair growth
126 on mouse incisors (Fig. 1b)[28]. As hair growth on the skin depends on multiple cell
127 populations arranged to form hair follicles (Fig. 1a, bottom), the question arises on how
128 hair development is achieved in a dental environment. Therefore, we evaluated the
129 cellular process leading to hair development in *Med1* cKO incisors by comparing it with
130 physiological hair in skin. Although hair grown on incisors of our mouse model shows an
131 almost the same hair architecture (cuticles), composition (coat and zig-zag hair) and
132 morphology as naturally grown skin hair (Fig 1b), hair formation significantly differs on
133 incisors. In fact, while skin grown hair is regenerated from large anagen follicles in
134 response to signals from the dermal papilla and maintained by small telogen follicles (Fig
135 1c, bottom orange arrows), we found that hair is supported by SI derived atypical cell
136 clusters without typical hair follicle-like structures at 4 wk of *Med1* cKO incisors (Fig. 1c
137 dotted lined region, and Suppl. Fig. 1c-e), when hair is first visible. These abnormal cell

138 clusters were originated from disorganized SI layer (Suppl. Fig. 1b red arrows) that are
139 progressed into expanded papillary layers (Suppl. Fig. 1c) to form hair bases in
140 mesenchymal tissues (Suppl. Fig. 1e). Hair differentiation was conducted by Notch1
141 positive SI/SR derived papillary cells form unusual cell aggregates and express the hair
142 marker keratin 71 (*Krt71*) at 4wk at maturation stage (Suppl. Fig 1d). Later at adult stages
143 after 3 months, these aggregates formed aberrant pocket-like structures (Fig. 2a).
144 Although these Notch1 expressing SI/SR derived cell clusters give rise to hair growth and
145 are rich in hair Krt71 expressing cells as well as in cells expressing the epidermal marker
146 Loricrin (Lor) (Fig. 2 a, b), the spatial organization of these cells is scattered and randomly
147 distributed (Fig 2b two left panels, blue arrows). This clearly differs from the well-defined
148 cellular framework found along hair follicles and on the surface of interfollicular epidermis
149 in the skin (Fig 2b, right panels, orange arrows). Furthermore, hair depilation on skin
150 initiates the hair follicle cycle by stimulating the growth of hair follicles (anagen) (Fig 2c
151 left 3 panels, blue arrows) and inducing the expression of *Krt31* (Suppl. Fig. 2a tooth). In
152 contrast, dental hair depilation did not activate any follicle-like structures in the hair
153 supporting tissues on *Med1* null incisors (Fig 2c two right panels, blue arrows) in either
154 distal or proximal incisor regions (Suppl. Fig. 2b) nor is the induction of the hair marker
155 *Krt31* (Suppl. Fig 2a). Nevertheless, hair grows back at its original length 12 days after
156 depilation in *Med1* cKO incisors (Fig 2d blue arrows), as occurs in normal skin (Suppl.
157 Fig. 2c).

158 These results demonstrate that hair can grow and is regenerated through SI
159 derived dental epithelia in a skin-extrinsic environment even in the absence of well-
160 organized hair follicle structural features (Fig. 2e) and without activation of the hair cycle.

161 Expression of hair and epidermal markers in the hair generating cell aggregates further
162 indicates that the presence of certain transcriptional patterns allow for the generation of
163 hair via a primitive cellular environment.

164 ***Med1* deficiency is sufficient to switch the dental transcriptional program towards**
165 **hair and epidermis in incisors *in vivo*.**

166 Cell identity and cell lineage progression tightly associate with a timed expression of
167 specific gene-sets. As loss of *Med1* causes hair growth in the dental compartment, using
168 total gene expression datasets we investigated the expression patterns of epidermal and
169 hair related gene sets at distinct anatomical locations of mouse incisors in *Med1* cKO
170 incisor (Fig. 3a, diagram). Our analyses revealed that compared to control mice, in *Med1*
171 cKO mice certain epidermal genes are already induced in the DE-SCs containing CL
172 region at 4 weeks of age (Fig 3b left panel, blue dotted box). Subsequently, as DE-SCs
173 differentiate towards the secretory (Sec) and maturation (Mat) stages, expression of many
174 epidermal genes strongly increases in *Med1* deficient tissue (Fig 3b). Intriguingly, hair
175 related genes are not yet detected in the CL locus but become clearly upregulated
176 downstream in the Sec and Mat regions (Fig 3b right panel). Immunostaining confirmed
177 the sequential induction of epidermal and hair markers as the epidermal markers Lor and
178 Krt1 were detected at secretory stage[29] but Krt71 was expressed only at maturation stage
179 (Suppl, Fig. 1d). These data illustrate how the expression of selected gene-sets during
180 dental hair development in cKO mice parallels embryonic and postnatal skin development
181 in wild type mice where epidermal development occurs first (E15), followed by hair follicle
182 formation (E18) (Fig. 3c). These results demonstrate that *Med1* deficiency is sufficient to

183 implement epidermal and hair related transcriptional programs priming dental stem cells
184 towards skin epithelial differentiation *in vivo*.

185 **Loss of *Med1* causes epidermal differentiation of DE-SCs *in vitro*.**

186 As the local microenvironment significantly influences adult stem cell differentiation *in*
187 *vivo*[3,6,9], the question arises as to the cellular and molecular mechanisms enabling the
188 tissue extrinsic differentiation shift of DE-SCs upon loss of *Med1*. To investigate this
189 phenomenon, DE-SCs containing CL tissues were dissected from 8-10 weeks old control
190 and *Med1* cKO mice and digested, then subsequently cells were plated and cultured until
191 self-renewing stem cell colonies formed *in vitro* (Fig. 4a). An enhanced proliferation rate
192 was observed for the *Med1* deficient cells as shown by the increased number of BrdU
193 positive cells as well as by the generation of larger colonies (Fig. 4b, cKO). Confirming
194 and expanding these results, IPA (ingenuity pathway analysis) of whole transcriptomic
195 data from these cultures not only revealed an upregulation of cell growth and proliferation
196 related pathways in *Med1* null cells, but also showed that these cells spontaneously
197 differentiate into the epidermal lineage in monolayer (Fig. 4c, d), even if the cell culture
198 was lacking mesenchymal feeder cells to induce epidermal differentiation. In fact, like Sec
199 tissue from cKO mice, an extensive set of epidermal related genes are clearly upregulated
200 in cultured *Med1* null DE-SCs as well (Fig. 4d). Of note, in line with our *in vivo* data above,
201 genes related to hair differentiation are only partially induced *in vitro*, suggesting that full
202 hair differentiation requires additional external processes. Furthermore, IPA analysis also
203 identified members of the p53 family (Tp63/53/73) as top upstream inducers of epidermal
204 differentiation (Fig. 4e) that are linked to the key epidermal AP-1 transcription factors *Fos*
205 and *Jun* (Fig. 4f). Collectively, these results show that epidermal commitment of *Med1*

206 null DE-SCs is directed by mechanisms which are independent from factors present in
207 their homing tissue. In consequence this suggests that upon loss of *Med1*, intracellular
208 mechanisms intrinsically reprogram the DE-SCs towards interfollicular epidermal
209 lineages.

210 **Med1 directly regulates the expression of enamel lineage driving transcription**
211 **factors by associating with their cis and trans regulatory elements.**

212 As part of the Mediator complex, Med1 associates with promoters and super-enhancers
213 (SEs), that are postulated to determine cell identity and properties as SEs induce
214 transcription of cell fate specific genes much higher than typical enhancers (TE)[38]. In our
215 mouse model, loss of *Med1,* shifts the lineage fate of dental epithelia towards hair
216 development. Therefore, to better understand the role of Med1 during DE-SC lineage
217 commitment and progression, we assess the genome wide distribution of Med1 and Med1
218 containing enhancers during dental epithelial development in control mice (4wk). We then
219 identify the enamel lineage specific TFs that are controlled by Med1/SE because TFs
220 primarily specify cell fate and capable to re-program cell lineages. For this purpose, we
221 performed Med1 ChIP-seq on the stem cell containing head region of the CL (CLH) as
222 well as on CL tail area (CLT) which includes their progenies (Fig. 5a, diagram). Med1 was
223 distributed in promoters and enhancers in distal intergenic regions in CLH and CLT (Suppl.
224 Fig. 3a). Subsequent enhancer analysis identified 325 SEs in the CLH region and 871
225 SEs in the CLT (Fig 5b, Suppl Fig 3b). These analyses identified a list of TFs (Fig 5d), in
226 which Med1 is recruited in their SEs. In the CLH tissues, SE locate near enamel lineage
227 TFs including *Pitx2*, *Isl1, and Nkx2-3* (Fig 5b left panel, Fig 5c left 3 panels). In contrast,
228 in CLT samples, SE are found around key TFs like Satb1 homeobox 1 (*Satb1)* and Runx

229 family transcription factor 1 (*Runx1*) and 2 (*Runx2*) which control later cellular processes
230 like differentiation and enamel mineralization (Fig. 5b right panel, Fig 5c right 3 panels).
231 Of note, the mRNA expression levels of these TFs are strongly reduced *Med1* cKO at
232 CLT (Fig. 5e), indicating their essential role for enamel formation because *Med1* null mice
233 show severe enamel dysplasia. In addition, Med1 levels are strongly enriched around the
234 promoters of these TFs while mature ameloblast markers shows only a slight increase in
235 Med1 levels when compared to the average of the genes. These results indicated that
236 Med1 directly activates these enamel fate TFs rather than supporting late differentiation
237 (Suppl Fig 4a). Intriguingly, we also found Med1 is recruited into enhancer region (SE or
238 TE) for another set of TFs (Fig. 5f), which are up regulated upon *Med1* loss in CLT tissues
239 (Fig. 5g). This set consists of genes involved in epidermal differentiation of the skin
240 including early growth response (*Egr3)*, CCAAT enhancer binding protein β (*Cebpb*), Fos
241 like 2 (*Fosl2*) (AP-1 transcription factor subunit), Kruppel like factor 3 (*Klf3*), Forkhead box
242 C1 (*Foxc1*), *Foxo3*, tumor protein Tp63, and hair fate driving factors like *Hr* and *Rin2*.
243 These data indicate that Med1 programs DE-SCs and their progenies to commit and
244 progress enamel lineage through critical TFs (Fig 5d). Lack of *Med1* may initiates
245 developmentally related epidermal fate presumably through epidermal driven TFs
246 enhancers (Fig 5f) that are present dental epithelia.

247 **Med1 deficiency reshapes the enhancer landscape in DE-SCs and their progenies.**
248 As loss of *Med1* inhibits the expression of Med1 associated enamel lineage driving TFs
249 but induces epidermal TFs in CL tissues, we next probed if this is linked to changes in
250 promoter and enhancer patterns upon loss of *Med1*. To test this hypothesis, we
251 performed ChIP-Seq analysis against the alternative enhancer marker histone 3 lysine

252 27 acetylation (H3K27ac) in CLH and CLT tissues of 4-week-old *Med1* cKO and their
253 littermate control mice (Fig. 6a). H3K27ac generally co-localizes with Med1 at distal
254 regulatory elements like typical enhancers (TE) and SEs and acts as a major inducer of
255 gene expression by increasing chromatin accessibility[38,40] as we have confirmed (Suppl.
256 Fig 4b). GREAT based GO analysis evidenced that in the CLT region, differential
257 H3K27ac peaks were associate with genes linked to enamel mineralization and tooth
258 morphogenesis (Fig. 6b blue bars), and epidermal and hair development (yellow bars).
259 We also found that these H3K27ac peaks are recruited in promoter regions for hair
260 lineage genes, epidermal genes in cKO in both CLT and CLH (Suppl. Fig. 5a). In contrast,
261 *Med1* deletion substantially increases the number of H3K27ac SEs (Fig. 6c) and TEs
262 (Suppl. Fig. 4c) in both, CLH and CLT. These new TEs and SEs are found around loci
263 coding for epidermal genes while in CLT tissues we observe an increased TE and SE
264 formation around hair lineage driving genes as well (Fig 6d), that are upregulated in Med1
265 cKO. For example, new H3K27ac marked SE was formed in epidermal driven Fosl2 (Ap-
266 1 factor) loci in cKO (Fig 6d blue bar in boxed region), linking to its mRNA induction in
267 *Med1* cKO (CLT) (Fig 5g), in which the locations of SE and TE are separately shown
268 (Suppl. Fig 5b). Moreover, when compared to the conserved and the newly formed SE at
269 CLT, GO terms show relatively low significance, suggesting that loss of Med1 increases
270 and expands SE occupancy around loci with pre-existing SEs (Suppl. Fig 4d).
271 Corroborating these results in line with our results from Fig. 4, we also found that the TF
272 binding motifs for the epidermal inducible TFs Tp53/63, Egr1 and AP-1 are significantly
273 enriched in cKO SEs compared to controls at CLT (Fig 6e). Collectively, loss of *Med1*
274 alters the epigenetic landscapes in DE-SCs and their progenies which are linked to

275 biological processes and pathways upstream of or extrinsic to DE-SCs and their
276 progenies. Our analyses also identify Med1 as check point factor which allocates lineage
277 specific epigenetic for ectoderm epithelia.

278 **Lack of *Med1* leads to H3K27ac signal amplification at epidermal and hair loci with**
279 **common occupancy profiles.**

280 Our results implicate that Med1 cKO utilizes developmentally conserved epidermal
281 enhancers present in dental epithelia. As dental and skin epithelia are derived from the
282 same ectoderm, we tested if two populations share common enhancer profiles around
283 epidermal and hair driven TFs. We found that even though dental epithelia usually do not
284 commit to epidermal fates, enhancer profiles are very similar round several key hair and
285 epidermal TFs in dental and skin epithelia. For examples, H3K27ac broad peaks
286 representing TE were present in control dental cells for epidermal fate driven Fols2 (Ap-
287 1 factor) (Fig. 7a red arrows, Suppl. Fig 5b), hair factors Hr (hairless) and Rin2 (Suppl.
288 Fig 5c). These enhancers were even shared in epidermal keratinocytes that were isolated
289 from normal mouse skin (10wk, telogen) (Fig 7a, b green), as well as in hair follicle
290 transient amplifying cells driving hair differentiation[41] (Fig 7a, b light blue, Suppl. Fig 5c
291 yellow). Similar results were obtained for other epidermal TFs, *Cebpb, Foxo3* (Suppl. Fig
292 6a) in which pre-existing TE/SE are expanded in cKO. In addition, enhancers were widely
293 shared in dental (CLH, CLT) and skin epithelia (epidermis and hair) for most of the *Med1*
294 cKO upregulated TFs (Fig 7c). Importantly, these H3K27ac marked enhancers were
295 elevated and upgraded into transcriptionally active SEs or expand in size (CLT, Fig 7a, b
296 SEs shown by blue bars, Suppl. Fig 6a) when *Med1* is lost.

297 Integrative analysis of H3K27ac Chip-seq data with RNA-seq based gene-set enrichment
298 analysis (GSEA) for CLH and CLT tissues (Suppl. Fig 7a) allowed us to further link the
299 epigenetic and transcriptional changes which lead to ectopic hair generation on incisors
300 upon loss of *Med1*. In addition to dental related components (Suppl. Fig 7d) and skin
301 epidermal differentiation genes (Suppl. Fig. 7e), we observed positive expression
302 enrichments for gene-sets involved “hair lineage genes” (Supple. Fig 7b) and negative
303 enrichments for gene-sets controlling “negative regulation of ossification” (Suppl. Fig. 7a
304 arrows). Many TFs found around “hair lineage genes” were elevated to SEs upon the loss
305 of *Med1* in CLT (Fig. 7d and Suppl. Fig. 5c, Suppl. Fig 6b). Intriguingly, these factors
306 controlling hair lineage were shown to be regulated by SE in the skin before[4]. Besides the
307 generation of new SEs, we also found a strong increase in H3K27ac levels around the
308 promoters (+/- 10kb from TSS) of these genes (Fig. 7e) in *Med1* null CLT tissues
309 potentially indicating activation of gene transcription via enhancer-promoter looping. In
310 fact, enhanced H3K27ac promoter levels positively correlate with an increased
311 expression of several members of the “hair lineage genes” (Fig. 7f) further confirming the
312 link between the generation of new SEs, activation of the SE-dependent hair lineage
313 genes and hair growth on *Med1* null incisors. Accordingly, in *Med1* cKO CLH tissues,
314 increased H3K27ac promoter levels positively correlate with an elevated expression of
315 genes involved in “negative regulation of ossification” (Suppl. Fig. 6c) and H3K27ac
316 occupancy increased in ossification regulated TFs of *Sox9* and *Tob1* loci in their
317 enhancers (Suppl Fig 6a). This further corroborates the dental phenotype of our mouse
318 model which is not only characterized by hair growth but also by enamel dysplasia.

319 In summary, we propose an epigenetic model in which *Med1* safeguards enamel lineage
320 specific epigenome in dental stem cells and progenies. *Med1* deletion initiates enamel-
321 to-hair lineage conversion by expanding the enhancer landscapes which causes the
322 formation of new SEs around hair and epidermal driven genes. These observations
323 positively correlate with an increased expression of hair and epidermal lineage driving
324 factors leading ultimately to hair development in dental tissues.
325

326 **DISCUSSION**
327
328 Adult stem cell fate is heavily linked to their tissue of origin[2,3,9]. It is postulated that the
329 local cellular and endocrine microenvironment primes and directs tissue specific lineage
330 commitment and differentiation via cellular, transcription and epigenetic mechanisms[2,4].
331 Here we show that deletion of *Med1*, a key component of enhancer associated Mediator
332 complex, causes ectopic hair growth on incisors. Unlike hair growth in the skin which
333 relies on functionally structured follicles, hair is generated from primitive, cellular
334 aggregates without hair follicle morphogenesis in a dental cellular environment.
335 Furthermore, as shown by our depilation experiments, dental hair regrows without
336 induction of the hair cycle, a follicle dependent process required for regeneration of hair
337 in the skin. Thus, our results question the current knowledge that mammalian hair can
338 only be generated from hair follicles consisting of multiple cell layers bearing bespoken
339 functions. In addition, our study also illustrates how deletion of Med1 induces an atypical
340 differentiation program in an extrinsic environment *in vivo*. Despite the cellular
341 agglomerates causing hair growth on incisors exhibit a scattered cellular setup, the mRNA
342 expression profiles found in these structures mimic those of dedicated hair and epidermal

343 cells found in skin epithelia. Thus, while Med1 negative DE-SCs reside in the dental
344 environment, they are driven towards lineages characteristic for skin epithelia.
345 Interestingly, loss of Med1 leads to differentiation into epidermal lineages in SI derived
346 cells, implicating their multi-potency of SI cells consistent to a previous study [42].

347 Lineage commitment and differentiation are orchestrated by epigenetic programs
348 and regulatory elements including TEs and SEs [4,38,40]. Our results elucidate that already
349 at early dental differentiation stages Med1 containing SEs selectively populate genomic
350 loci coding for enamel fate driven TFs in DE-SCs and their progenies. This outlines how
351 Med1 controls and programs enamel epithelia's differentiation at multiple stages as it
352 primes DE-SCs towards the dental lineage via activation of *Nkx2-3, Pitx2* and *Isl1* and
353 calibrates lineage progression of DE-SC progenies by regulating the expression of
354 *Runx1/2* and *Satb1.* These findings are consistent with previous studies that *Nkx2-3*
355 controls cusp formation in embryonic dental epithelia[24], and *Nkx2-3, Pitx2 and Runx2* as
356 essential for dental development[24,43,44]. *Isl1* is required for patterning and mineralization
357 of enamel[25], Runx2 for enamel mineralization [45,46], and *Satb1* for cell polarity and enamel
358 matrix secretion in amelogenesis[47].

359 Intriguingly, although Med1 is a well-recognized SE component, loss of *Med1* in
360 CL tissues does not compromise SE formation but significantly widens the genomic
361 enhancer landscape instead. In the dental setting, this does not increase the potency on
362 DE-SCs but rather drives these cells into epidermal linages. This coincides with a shift in
363 the SE profiles around loci coding for TFs like *Hr* (hairless) and *Rin2* which are essential
364 for hair formation[26,27] as well as *Egr1/3, CEBP/a*, *CEBP/b*, and *Fosl2* which control
365 epidermal differentiation at different stages[48,49]. Furthermore, our data show that the

366 *Med1* null SE are enriched in Tp63/53 binding sites. They are master regulators for the
367 development of stratified epithelia *in vivo*[19] and drive epidermal differentiation of *Med1*
368 null stem cells *in vitro*. In fact, *Med1* null mice activate Tp63 driven epidermal
369 differentiation in the skin, in which epidermal markers and lipids are accumulated in upper
370 hair follicle keratinocytes resulting in hair loss[28].

371 Building on our previous studies[29], these results elucidate a central role for Med1
372 in assuring tissue specific lineage differentiation of adult stem cells into enamel producing
373 dental epithelia. Our results also reveal that basal H3K27ac levels are already found at
374 hair and epidermis driven TFs related loci in control DE-SCs suggesting that a basal
375 epigenetic memory granting multipotency is already established in pre-occurring
376 ectoderm during embryonic development. Consequently, in post-natal tissues, Med1
377 guarantees adult stem cell commitment and differentiation into tissue intrinsic lineages by
378 restricting SE formation to selective and lineage specific loci. In addition, as loss of *Med1*
379 causes DE-SCs to differentiate into a developmentally related lineage might indicate that
380 DE-SCs trans-differentiation into lineages originating from different germ layers would
381 probably need overcoming of more strict and embryonically set epigenetic barriers[38].

382 Hair as well as enamel are tissues which under certain conditions are difficult to
383 regenerate. A deep understanding of the cellular and epigenetic mechanisms controlling
384 the formation of these tissues creates new entry points for the development of strategies
385 to combat skin, hair, and tooth related diseases. Our results establish that hair formation
386 is achievable in tissue other than the skin, even without the presence of hair follicles.
387 Similarly, hair was also accidentally generated by DE-SCs transplanted into renal
388 capsules during an effort to regenerate enamel[50]. This suggests that hair could be

389 generated via genetically engineered cell clusters or organoids *in vitro* which might be
390 easier than traditional strategies and bypass time consuming re-programming processes.
391 This would be of great benefit as it would greatly simplify *in vitro* hair generation and allow
392 hair growth without hair follicles which are very challenging to regenerate[51]. Similarly,
393 enamel regeneration might also be feasible by using foreskin derived epidermal stem
394 cells. In fact, cultured epidermal stem cells derived from skin have been shown to
395 differentiate into functional ameloblasts *in vitro*[52]. Overall, these findings, elucidate novel
396 possibilities to develop strategies to overcome hair and enamel associated diseases.
397

398 **MATERIALS AND METHODS**

399

400 **Krt14-driven *Med1* cKO mice**

401 Conditional *Med1* knockout (cKO) mice were generated as described previoulsy[28]. Floxed
402 (exon 8-10) *Med1* mice[53] (C57/BL6 background) were mated with keratin 14 (Krt14)
403 promoter driven *Cre* recombinase mice (The Jackson Laboratory, C57/BL6 background).
404 Genotyping was performed by PCR as previously described[28] and *Cre* negative littermate
405 mice served as controls (Ctrl). All the experiments were approved by the Institutional
406 Animal Care and Ethics Committee at the San Francisco Department of Veterans Affairs
407 Medical Center.

408 **Histological analysis**

409 Mouse mandibles were dissected from *Med1* KO and littermate control (CON) mice and
410 fixed in 4% paraformaldehyde at 4°C for overnight and decalcified in 0.5 M EDTA for two
411 weeks. Subsequently they were dehydrated and embedded in paraffin wax using

412 standard protocols. The whole mandible was then serially sectioned at 7 μm (sagittal
413 sections) containing both the CL and enamel organ. Ultimately, slides were stained with
414 hematoxylin and eosin (HE) and imaged with brightfield microscopy.

415 **Immunostaining**

416 For immunostaining, paraffin embedded jaw sections were treated with antigen
417 unmasking solutions (Vector lab Citrate-based, H-3300) and subsequently blocked with
418 an avidin/biotin blocking solution (Vector lab, SP-2001) and incubated with primary
419 antibodies against Krt71 (Covance), Notch1 (Cell Signaling) and Loricrin (Covance). They
420 were then developed by Vectastain Elite ABC kit (Vector Lab) using DAB staining solution
421 (Vector Lab, SK-4100) until brown signals were visible. The sections were counterstained
422 with Gill's Hematoxylin.

423 **Immunofluorescence**

424 Paraffin-embedded mandible sections were pretreated in 10 mmol/L citrate buffer (pH 6.0,
425 Sigma-Aldrich) for 20 min using a microwave for antigen retrieval. The specimens were
426 blocked by Power Block (BioGenex) and incubated with primary antibodies against Krt71
427 (Progen), Krt1, (Covance), Loricrin (Covance) and Notch1 (Cell signaling). They were
428 subsequently incubated with species specific secondary antibodies conjugated with
429 fluorescent dyes (Invitrogen Molecular probes), including Alexa 594 (red) and Alexa 488
430 (green), and counterstained with DAPI. Images were taken with a confocal microscope
431 (LSM510, Carl Zeiss).

432 **Dental epithelial stem cell (DE-SC) culture**

433 CL tissue was separated from 10 wk *Med1* KO and CON mice, and epithelial tissues were
434 separated and treated by dispase (5U/ml Stem Cell Technology) to separate
435 mesenchymal tissues. Epithelial tissues are further dissociated by accutase (Sigma
436 Milipore), and cells were plated under low density to generate colonies and maintained
437 with DMEM media supplemented with recombinant EGF 20 ng/ml (R&D), FGF 25 ng/ml
438 (R&D), 1X B27 supplement (Gibco). After 8 days of culture, number and size of colonies
439 are evaluated, and RNA is prepared for microarray.

440 **BrdU staining**

441 DE-SC are labeled by BrdU and stained by a BrdU staining kit (Abcam) by following
442 manufacturer's instruction.

443 **Chromatin immunoprecipitation**

444 Chromatin IP was performed by using the LowCell# ChIP kit (Diagenode) for H3K27ac,
445 and the iDeal ChIP-kit (Diagenode) for Med1 according to the manufacturer's protocols
446 with some modifications as described below. Dissected CLH or CLT tissues were cross-
447 linked with 1% paraformaldehyde for 8 min (H3K27ac) or for 15 min (Med1) and
448 subsequently quenched with 0.125M glycine. Epidermal keratinocytes containing stem
449 and proneny were isolated from mouse skin were fixed with 1% paraformaldehyde for 10
450 min. Chromatin was then sonicated with a Covaris S2200 ultra-sonicator (Covaris, Inc.)
451 to obtain DNA fragments with an average length of 300±50 bp. The fragment size was
452 verified with an Agilent 2100 Bioanalyzer (Agilent Technologies). Sheared chromatin was
453 thereafter immunoprecipitated with Protein A-coated magnetic beads (Diagenode)
454 preincubated with 4.5 μg/IP Med1 antibody (Bethyl A300-793A) or 3 μg/IP H3K27ac

455 antibody (ab4729, Abcam). Chromatin input samples were used as reference. Complexes
456 were then washed and eluted from the beads with washing buffer and crosslinks were
457 reversed by incubation with proteinase K at 65°C for 4 hours. Immunoprecipitated DNA
458 along with genomic DNA (Inputs) were purified using the IPure v2 kit (Diagenode). IP
459 efficiency was confirmed by qPCR using primers provided in the kits. Experiments were
460 carried out in duplicates. ChIP-Seq libraries were generated using the Accel-NGS 2S Plus
461 DNA library kits (Swift Sciences) and amplified by PCR for 11-13 cycles. High molecular
462 weight smear was removed in the library by right side size selection using SPRI beads
463 (Beckman Coulter). The libraries were quantified by Agilent 2100 Bioanalyzer with the
464 high sensitivity DNA assay and sequenced on an Illumina HiSeq 4000 (UCSF Center of
465 advanced technology) in a single strand 50 bp run.

466 **RNA expression analysis**

467 Total RNA was isolated from 4-week-old total CL, CLH, CLT, Sec or Mat tissues of *Med1*
468 cKO and littermate Ctrl mice using the Pico Pure RNA purification kit (ABI). RNA from
469 cultured dental epithelial stem cells was extracted using the RNeasy mini kit (Qiagen).
470 RNAs were analyzed for quality and purity using the Pico Chip on an Agilent 2100
471 Bioanalyzer (Agilent Technologies) to meet the processing criteria of the UCLA Genomic
472 Core facility for the Illumina array platform (Mouse Ref-8 v2.0 Ambion) or RIN score
473 values for RNA-seq. Microarray data generation and primary microarray data analysis
474 was described previously [12]. Microarray data was used for differential pathway analysis
475 with Ingenuity IPA software (Ingenuity) and results were considered significant for *p*-
476 values less than 0.005. Heat maps were then generated with MeV software using fold
477 changes (cKO/Ctrl). For RNA-Seq analysis, RNA integrity was analyzed with a 2100

478 Bioanalyzer with an RNA 6000 kit (Agilent Technologies). RNA-Seq libraries were
479 prepared using the Illumina TruSeq v2 library preparation kit and sequenced with paired-
480 end 50 bp reads on an Illumina HiSeq 4000 in biological duplicates.
481 For quantitative real-time polymerase chain reaction (rt-qPCR), cDNA was synthesized
482 from ~0.5 µg RNA using the SuperScript III first strand synthesis system (Invitrogen) as
483 described by the supplier and subjected to rt-qPCR amplification using the QuantiTect
484 SYBR-Green PCR Kit (Qiagen) and a 7300 or 7500 Real Time PCR system (Applied
485 Biosystems) using the following conditions: 10 min 95°C followed by 45 cycles of 30 sec
486 at 95°C, 30 sec at 60°C and 30 sec at 72°C. Relative mRNA levels compared to the
487 housekeeping gene *Gapdh* and determined with the ΔΔCt method. Primers for the
488 analyzed genes are provided upon requests. All rt-qPCR assays were performed in
489 triplicates.
490 **Next generation DNA sequence data analysis**
491 For RNA-Seq data analysis, raw reads were assessed for run quality using fastqc version
492 0.72 followed by alignment to reference genome (mm10) using RNA STAR Galaxy
493 version 2.6.0b-1 with default settings. Differential gene expression analysis was
494 performed using featureCounts Galaxy version 1.6.3 and DESeq2 Galaxy version
495 2.11.40.2. For ChIP-Seq data analysis, raw reads from Med1 or H3K27ac ChIP-seq
496 sequencing experiments were assessed for quality using fastqc version 0.72, followed by
497 mapping to reference genome (mm10) using BWA Galaxy version 0.7.15.1 with standard
498 settings. Pooled peak calling was performed with MACS2 callpeak version
499 2.1.0.20140616.0 using broad peak settings and a minimum FDR cutoff of 0.05. Raw-
500 files for publically available H3K27ac ChIP-Seq datasets from wildtype mice hair stem

501 cell progenies were downloaded from the NCBI-SRA database (SRR1573273,
502 SRR1573274) and analyzed as described above. To assess significantly different peak
503 occupancy between two experimental groups, peak files (MACS2) were analyzed with
504 DiffBind Galaxy version 2.6.6.4 or 2.10.0. Peak size and location were visualized with IGV
505 version 2.3.92.MAYO using group auto-scale for comparable visualization of all shown
506 groups. Peak intensity around TSS (±10 kbp) as well as genomic peak distribution was
507 assessed with CEAS software (Version1.0.0, Cistrome, Liu Lab). Gene-ontology analysis
508 for Med1 or H3K27ac distal intergenic cis-regulatory elements was performed using
509 GREAT version 3.0.0 (Bejerano Lab, Stanford). Super enhancer analysis was performed
510 using the ROSE package and the software NaviSE. Overlapping TE and SE between the
511 shown comparisons were assessed with Bedtools (version 2.29) using a minimum
512 overlap of 50%. Motif analysis (de novo and known) was performed using HOMER
513 software [32]. Curated gene-sets used for analyses in this study are provided upon
514 requests.

515 **Reproducibility and statistical analysis**

516 All the experiments using *Med1* cKO and littermate control mice (n=3) were repeated with
517 at least two litters, and reproducibility was confirmed. The experiments using cultured
518 dental epithelia were conducted in duplicates for microarray, and reproducibility was
519 confirmed. Histologic analyses were performed using 2 sections per mouse per each
520 group of cKO and CON, and representative images are shown. Statistical significance
521 was calculated using software integrated methods or two-tailed unpaired Student's t-test.
522 If not differently noted, differences with a *p*-value of less than 0.05 were considered as
523 statistically significant.

524 **Data availability**
525
526 The array data were submitted to a public database (GEO/NCBI/NIH
527 http://www.ncbi.nlm.nih.gov/geo). Data for *Med1* cKO (4wk), are available with accession
528 numbers GSE50672, GSE50671, GSE50670, respectively under the super-series
529 GSE50673. We are pending of RNA-seq and ChIP-seq data submission.
530

531 **AUTHOR CONTRIBUTIONS**
532
533 Conceptualization: Y.O., R.T., K.Y., S.F., P.D., D.D.B; Methodology: Y.O., R.T., T.N.,
534 K.Y.; Investigation: Y.O., R.T., T.N., K.Y.; Writing-Original Draft: Y.O. Writing-Review &
535 Editing: R.T., Y. O., S.F., P.D., D.D.B; Funding Acquisition: D.D.B., Y.O., S.F., K.Y.,
536 Resources: R.T., K.Y., S.F., D.D.B., Y.O.
537
538 **DECLARATION OF INTERESTS**

539 The authors declare no competing interests.
540

541 **ACKNOWLEDGMENTS**

542 We thank Ms Sun Hee Kim Wong for in maintaining the mice and technical assistance.
543 We are also grateful to L. Hu, C. Fong for technical supports. This work was supported
544 by the NIH grant R21 DE025357 (YO), R01 AR050023 (DDB), DOD grant CA110338
545 (DDB), VA Merit I01 BX003814-01 (DDB).
546

547 **REFERENCES**

548 1 Wabik, A. & Jones, P. H. Switching roles: the functional plasticity of adult tissue stem cells.
549 *EMBO J* **34**, 1164-1179, doi:10.15252/embj.201490386 (2015).
550 2 Garcia-Prat, L., Sousa-Victor, P. & Munoz-Canoves, P. Proteostatic and Metabolic Control
551 of Stemness. *Cell Stem Cell* **20**, 593-608, doi:10.1016/j.stem.2017.04.011 (2017).

3 Middendorp, S. *et al.* Adult stem cells in the small intestine are intrinsically programmed with their location-specific function. *Stem Cells* **32**, 1083-1091, doi:10.1002/stem.1655 (2014).
4 Adam, R. C. *et al.* Pioneer factors govern super-enhancer dynamics in stem cell plasticity and lineage choice. *Nature* **521**, 366-370, doi:10.1038/nature14289 (2015).
5 Kaltschmidt, B., Kaltschmidt, C. & Widera, D. Adult craniofacial stem cells: sources and relation to the neural crest. *Stem Cell Rev Rep* **8**, 658-671, doi:10.1007/s12015-011-9340-9 (2012).
6 Jimenez-Rojo, L., Granchi, Z., Graf, D. & Mitsiadis, T. A. Stem Cell Fate Determination during Development and Regeneration of Ectodermal Organs. *Front Physiol* **3**, 107, doi:10.3389/fphys.2012.00107 (2012).
7 Yoshizaki, K., Fukumoto, S., Bikle, D. D. & Oda, Y. Transcriptional Regulation of Dental Epithelial Cell Fate. *Int J Mol Sci* **21**, doi:10.3390/ijms21238952 (2020).
8 Bianco, P., Robey, P. G. & Simmons, P. J. Mesenchymal stem cells: revisiting history, concepts, and assays. *Cell Stem Cell* **2**, 313-319, doi:10.1016/j.stem.2008.03.002 (2008).
9 Wei, Y. *et al.* Human skeletal muscle-derived stem cells retain stem cell properties after expansion in myosphere culture. *Exp Cell Res* **317**, 1016-1027, doi:10.1016/j.yexcr.2011.01.019 (2011).
10 Wang, X. P. *et al.* An integrated gene regulatory network controls stem cell proliferation in teeth. *PLoS Biol* **5**, e159, doi:10.1371/journal.pbio.0050159 (2007).
11 Klein, O. D. *et al.* An FGF signaling loop sustains the generation of differentiated progeny from stem cells in mouse incisors. *Development* **135**, 377-385, doi:10.1242/dev.015081 (2008).
12 Mitsiadis, T. A. & Graf, D. Cell fate determination during tooth development and regeneration. *Birth Defects Res C Embryo Today* **87**, 199-211, doi:10.1002/bdrc.20160 (2009).
13 Fuchs, E., Tumbar, T. & Guasch, G. Socializing with the neighbors: stem cells and their niche. *Cell* **116**, 769-778, doi:S0092867404002557 [pii] (2004).
14 Juuri, E. *et al.* Sox2 marks epithelial competence to generate teeth in mammals and reptiles. *Development* **140**, 1424-1432, doi:10.1242/dev.089599 (2013).
15 Juuri, E. *et al.* Sox2+ stem cells contribute to all epithelial lineages of the tooth via Sfrp5+ progenitors. *Dev Cell* **23**, 317-328, doi:10.1016/j.devcel.2012.05.012 (2012).
16 Morita, R. *et al.* Tracing the origin of hair follicle stem cells. *Nature* **594**, 547-552, doi:10.1038/s41586-021-03638-5 (2021).
17 Gonzales, K. A. U. & Fuchs, E. Skin and Its Regenerative Powers: An Alliance between Stem Cells and Their Niche. *Dev Cell* **43**, 387-401, doi:10.1016/j.devcel.2017.10.001 (2017).
18 Sundberg, J. P., Peters, E. M. & Paus, R. Analysis of hair follicles in mutant laboratory mice. *J Investig Dermatol Symp Proc* **10**, 264-270, doi:10.1111/j.1087-0024.2005.10126.x (2005).
19 Botchkarev, V. A. & Flores, E. R. p53/p63/p73 in the epidermis in health and disease. *Cold Spring Harb Perspect Med* **4**, doi:10.1101/cshperspect.a015248 (2014).
20 Greco, V. *et al.* A two-step mechanism for stem cell activation during hair regeneration. *Cell Stem Cell* **4**, 155-169, doi:10.1016/j.stem.2008.12.009 (2009).
21 Alonso, L. & Fuchs, E. The hair cycle. *J Cell Sci* **119**, 391-393, doi:10.1242/jcs.02793 (2006).
22 Sakai, Y. & Demay, M. B. Evaluation of keratinocyte proliferation and differentiation in vitamin D receptor knockout mice. *Endocrinology* **141**, 2043-2049 (2000).
23 Lin, C. R. *et al.* Pitx2 regulates lung asymmetry, cardiac positioning and pituitary and tooth morphogenesis. *Nature* **401**, 279-282, doi:10.1038/45803 (1999).

24 Han, X. *et al.* The transcription factor NKX2-3 mediates p21 expression and ectodysplasin-A signaling in the enamel knot for cusp formation in tooth development. *J Biol Chem* **293**, 14572-14584, doi:10.1074/jbc.RA118.003373 (2018).
25 Naveau, A. *et al.* Isl1 Controls Patterning and Mineralization of Enamel in the Continuously Renewing Mouse Incisor. *J Bone Miner Res* **32**, 2219-2231, doi:10.1002/jbmr.3202 (2017).
26 Panteleyev, A. A., Paus, R., Ahmad, W., Sundberg, J. P. & Christiano, A. M. Molecular and functional aspects of the hairless (hr) gene in laboratory rodents and humans. *Exp Dermatol* **7**, 249-267, doi:10.1111/j.1600-0625.1998.tb00295.x-i1 (1998).
27 Basel-Vanagaite, L. *et al.* RIN2 deficiency results in macrocephaly, alopecia, cutis laxa, and scoliosis: MACS syndrome. *Am J Hum Genet* **85**, 254-263, doi:10.1016/j.ajhg.2009.07.001 (2009).
28 Oda, Y. *et al.* Coactivator MED1 ablation in keratinocytes results in hair-cycling defects and epidermal alterations. *J Invest Dermatol* **132**, 1075-1083, doi:10.1038/jid.2011.430 (2012).
29 Yoshizaki, K. *et al.* Ablation of coactivator Med1 switches the cell fate of dental epithelia to that generating hair. *PLoS One* **9**, e99991, doi:10.1371/journal.pone.0099991 (2014).
30 Yoshizaki, K. *et al.* Mediator 1 contributes to enamel mineralization as a coactivator for Notch1 signaling and stimulates transcription of the alkaline phosphatase gene. *J Biol Chem* **292**, 13531-13540, doi:10.1074/jbc.M117.780866 (2017).
31 Malik, S. & Roeder, R. G. Dynamic regulation of pol II transcription by the mammalian Mediator complex. *Trends Biochem Sci* **30**, 256-263, doi:S0968-0004(05)00081-2 [pii] 10.1016/j.tibs.2005.03.009 (2005).
32 Kornberg, R. D. Mediator and the mechanism of transcriptional activation. *Trends Biochem Sci* **30**, 235-239 (2005).
33 Taatjes, D. J. The human Mediator complex: a versatile, genome-wide regulator of transcription. *Trends Biochem Sci* **35**, 315-322, doi:S0968-0004(10)00025-3 [pii] 10.1016/j.tibs.2010.02.004 (2010).
34 Oda, Y., Chalkley, R. J., Burlingame, A. L. & Bikle, D. D. The transcriptional coactivator DRIP/mediator complex is involved in vitamin D receptor function and regulates keratinocyte proliferation and differentiation. *J Invest Dermatol* **130**, 2377-2388, doi:10.1038/jid.2010.148 (2010).
35 Yue, X., Izcue, A. & Borggrefe, T. Essential role of Mediator subunit Med1 in invariant natural killer T-cell development. *Proc Natl Acad Sci U S A* **108**, 17105-17110, doi:10.1073/pnas.1109095108 (2011).
36 Jiang, P. *et al.* Key roles for MED1 LxxLL motifs in pubertal mammary gland development and luminal-cell differentiation. *Proc Natl Acad Sci U S A* **107**, 6765-6770, doi:10.1073/pnas.1001814107 (2010).
37 Jia, Y. *et al.* Peroxisome proliferator-activated receptor-binding protein null mutation results in defective mammary gland development. *J Biol Chem* **280**, 10766-10773, doi:10.1074/jbc.M413331200 (2005).
38 Whyte, W. A. *et al.* Master transcription factors and mediator establish super-enhancers at key cell identity genes. *Cell* **153**, 307-319, doi:10.1016/j.cell.2013.03.035 (2013).
39 Zhang, X. *et al.* MED1/TRAP220 exists predominantly in a TRAP/ Mediator subpopulation enriched in RNA polymerase II and is required for ER-mediated transcription. *Mol Cell* **19**, 89-100, doi:10.1016/j.molcel.2005.05.015 (2005).
40 Hnisz, D. *et al.* Super-enhancers in the control of cell identity and disease. *Cell* **155**, 934-947, doi:10.1016/j.cell.2013.09.053 (2013).
41 Lien, W. H. *et al.* Genome-wide maps of histone modifications unwind in vivo chromatin states of the hair follicle lineage. *Cell Stem Cell* **9**, 219-232, doi:10.1016/j.stem.2011.07.015 (2011).

42 Sharir, A. *et al.* A large pool of actively cycling progenitors orchestrates self-renewal and injury repair of an ectodermal appendage. *Nat Cell Biol* **21**, 1102-1112, doi:10.1038/s41556-019-0378-2 (2019).
43 Cao, H. *et al.* The Pitx2:miR-200c/141:noggin pathway regulates Bmp signaling and ameloblast differentiation. *Development* **140**, 3348-3359, doi:10.1242/dev.089193 (2013).
44 D'Souza, R. N. *et al.* Cbfa1 is required for epithelial-mesenchymal interactions regulating tooth development in mice. *Development* **126**, 2911-2920 (1999).
45 Chu, Q. *et al.* Ablation of Runx2 in Ameloblasts Suppresses Enamel Maturation in Tooth Development. *Sci Rep* **8**, 9594, doi:10.1038/s41598-018-27873-5 (2018).
46 Xuan, D. *et al.* Effect of cleidocranial dysplasia-related novel mutation of RUNX2 on characteristics of dental pulp cells and tooth development. *J Cell Biochem* **111**, 1473-1481, doi:10.1002/jcb.22875 (2010).
47 Zhang, Y. *et al.* SATB1 establishes ameloblast cell polarity and regulates directional amelogenin secretion for enamel formation. *BMC Biol* **17**, 104, doi:10.1186/s12915-019-0722-9 (2019).
48 Kim, K. H. *et al.* EGR3 Is a Late Epidermal Differentiation Regulator that Establishes the Skin-Specific Gene Network. *J Invest Dermatol* **139**, 615-625, doi:10.1016/j.jid.2018.09.019 (2019).
49 House, J. S., Zhu, S., Ranjan, R., Linder, K. & Smart, R. C. C/EBPalpha and C/EBPbeta are required for Sebocyte differentiation and stratified squamous differentiation in adult mouse skin. *PLoS One* **5**, e9837, doi:10.1371/journal.pone.0009837 (2010).
50 Zheng, L. W., Linthicum, L., DenBesten, P. K. & Zhang, Y. The similarity between human embryonic stem cell-derived epithelial cells and ameloblast-lineage cells. *Int J Oral Sci* **5**, 1-6, doi:10.1038/ijos.2013.14 (2013).
51 Takeo, M. *et al.* Expansion and characterization of epithelial stem cells with potential for cyclical hair regeneration. *Sci Rep* **11**, 1173, doi:10.1038/s41598-020-80624-3 (2021).
52 Hu, X. *et al.* Efficient induction of functional ameloblasts from human keratinocyte stem cells. *Stem Cell Res Ther* **9**, 126, doi:10.1186/s13287-018-0822-4 (2018).
53 Jia, Y. *et al.* Transcription coactivator PBP, the peroxisome proliferator-activated receptor (PPAR)-binding protein, is required for PPARalpha-regulated gene expression in liver. *J Biol Chem* **279**, 24427-24434, doi:10.1074/jbc.M402391200
M402391200 [pii] (2004).

694 **FIGURES**

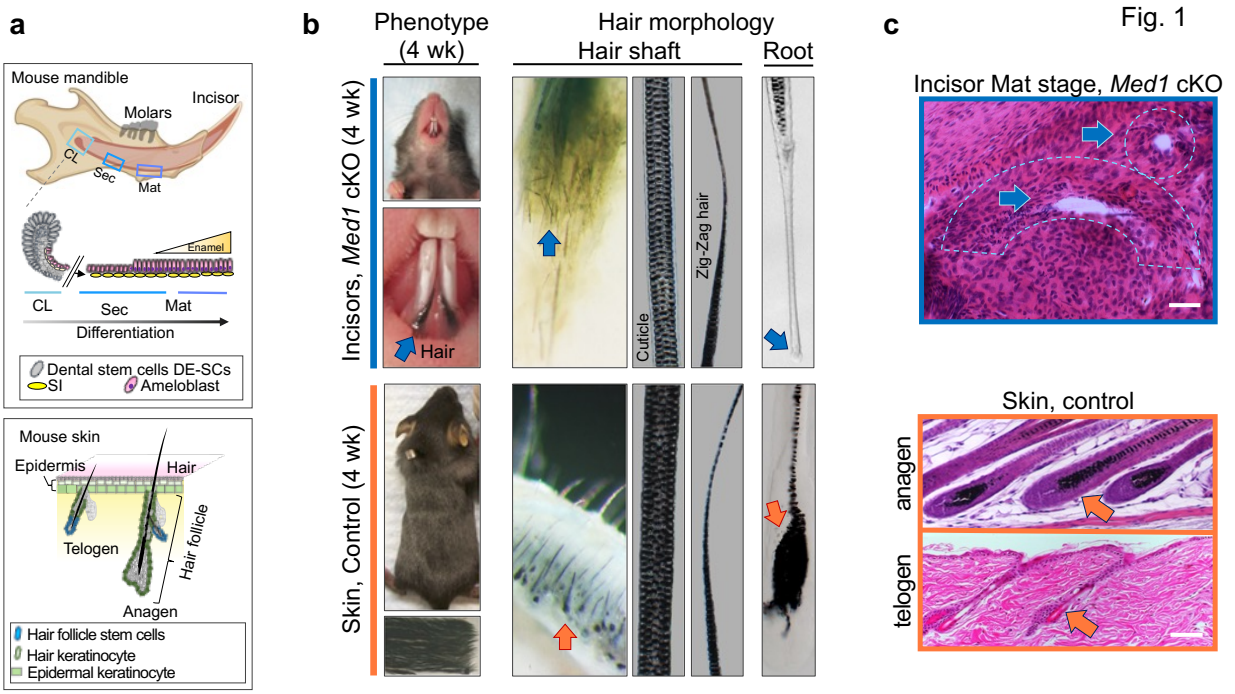

695

696 **Fig. 1: Loss of *Med1* in dental stem cells causes ectopic hair growth on incisors. a**
697 Top**,** Diagrams representing normal dental epithelial differentiation and enamel formation
698 in mouse mandible. CL, cervical loop; Sec; secretory stage; Mat, maturation stage; DE-
699 SCs, dental epithelial stem cells; SI, stratum intermedium. Bottom, Hair is regenerated
700 by hair follicles under cycling regulation of anagen and telogen in skin. **b** Hair growth on
701 *Med1* cKO incisors at 4 weeks of age (top) that has been consistently observed in over
702 60 generations of *Med1* cKO mice, is compared to normal hair in skin (bottom). **c** Top,
703 H&E sections supporting hair (blue arrows) in *Med1* cKO incisors at 4 weeks of age
704 (dotted lines. Bottom, H&E sections for hair follicles at anagen (top) and telogen phases
705 (bottom) supporting hair in skin. Bars = 25 μm. For (**b, c**), representative images are
706 shown.

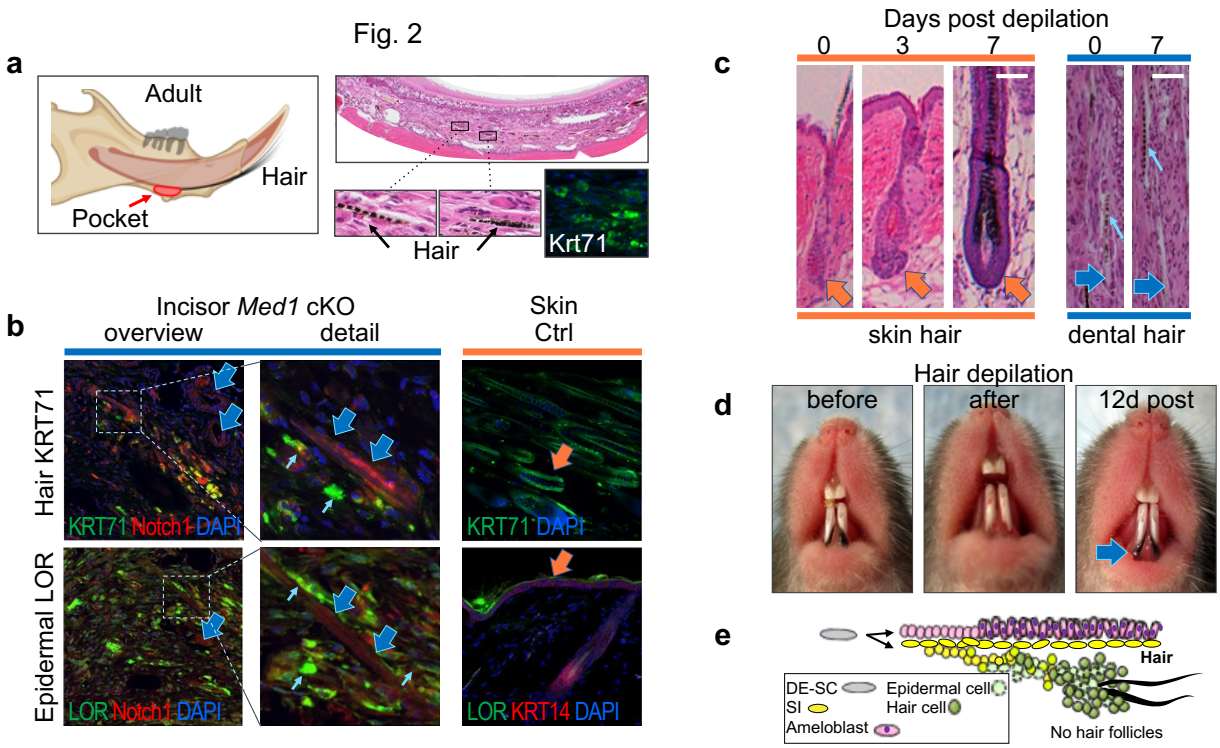

Fig. 2: *Med1* null incisors develop and regenerate hair without morphogenesis of hair follicles. **a** Left, diagram depicting hair generation via pocket-like structures (red) in *Med1* cKO incisors in adult mice. Right, H&E stain to show hair in dental tissues and immune-staining against hair marker Krt71 (green). **b** Top, immuno-staining of hair marker Krt71 (green) and Notch1 (red) in the pocket of *Med1* cKO incisors or of Krt71 only (green) in normal skin. Bottom, epidermal marker Lor (green) and Notch1 (red) in dental tissues compared to Lor (green) and Krt14 (red) localization the skin. Large blue arrows show auto-fluorescent hair structures. **c** H&E staining sections of skin (orange) and dental (blue) sections before (0 day) and after hair depilation (3 and 7 days). Small arrows show hair. Bars = 25 μm. **d** Full hair regeneration 12 days after hair depilation from *Med1* cKO mice. **e** Schematic representation of cellular process and anatomical location of dental SI/SR derived dental epithelia that are gradually transformed into epidermal (pale green) and hair gene expressing (green) aberrant cell aggregates without hair follicle structures in *Med1* cKO incisors. For all images, representative images are shown, and reproducibility was confirmed at least in two different litters of *Med1* cKO and control mice.

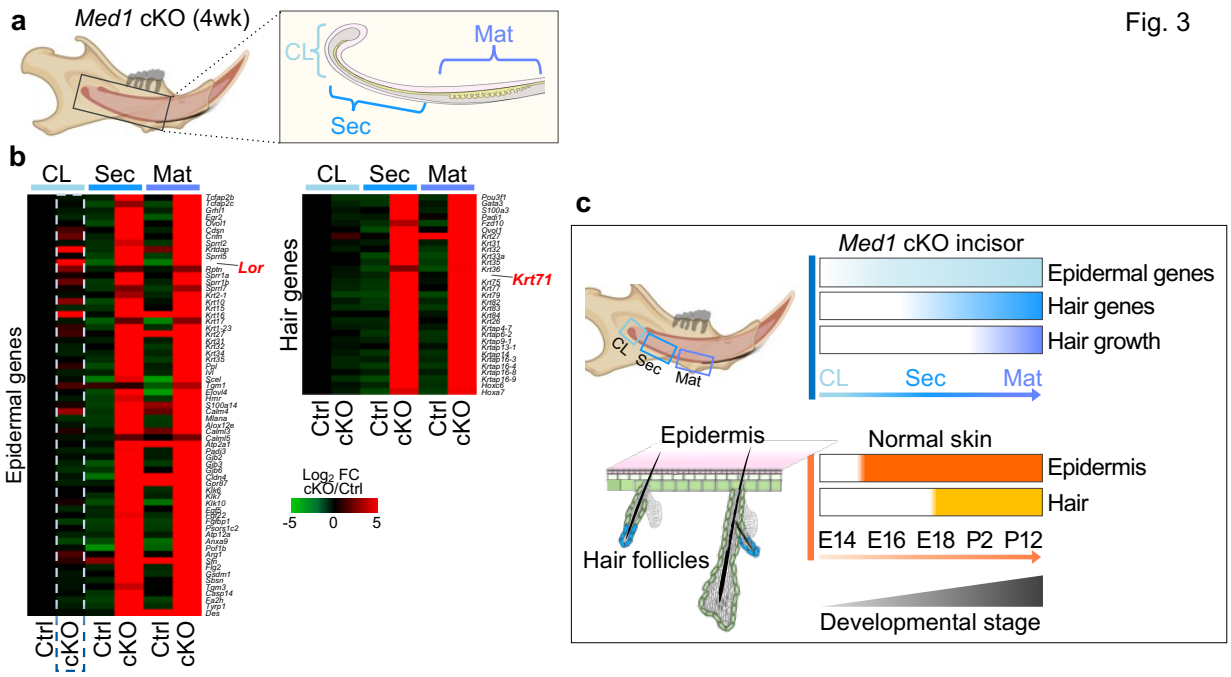

Fig. 3: Loss of *Med1* activates epidermal and hair gene expression in developing incisors. a Diagram depicting the anatomical locations in Ctrl and *Med1* cKO incisors. CL, cervical loop; Sec, secretory stage; Mat, maturation stage. **b** Heatmap showing differential gene expressions for epidermal genes (left) and hair genes (right) in *Med1* cKO incisors versus Ctrl at 4 weeks of age. For each gene, fold changes are compared to CL Ctrl; n=3 for all samples and average values for each group are shown. **c** Top, A diagram to show the hair growth (purple), hair genes (blue) and epidermal genes (light blue) are induced at different stages (CL, Sec and Mat) of *Med1* cKO incisors. Bottom, this pattern is synchronized to sequential inductions of epidermal (orange, E15), and hair genes (yellow, E18) arising during embryonic development of the skin.

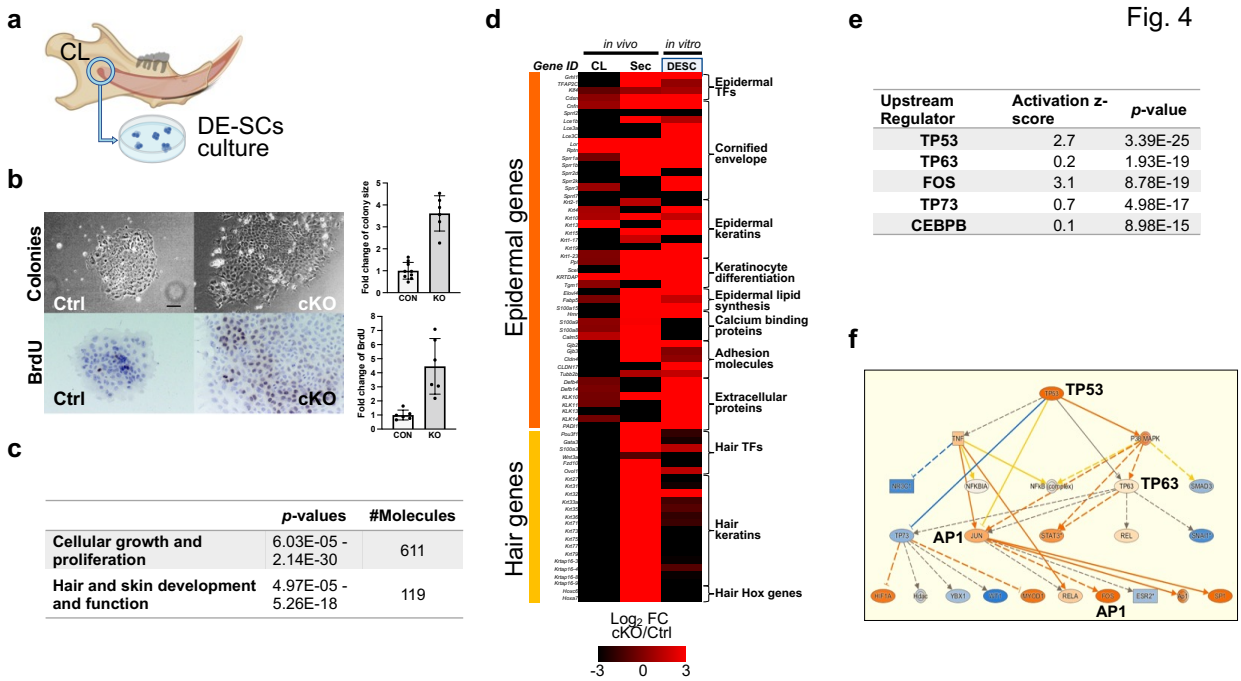

Fig. 4

	p-values	#Molecules
Cellular growth and proliferation	6.03E-05 - 2.14E-30	611
Hair and skin development and function	4.97E-05 - 5.26E-18	119

Upstream Regulator	Activation z-score	*p*-value
TP53	2.7	3.39E-25
TP63	0.2	1.93E-19
FOS	3.1	8.78E-19
TP73	0.7	4.98E-17
CEBPB	0.1	8.98E-15

Fig. 4: *Med1* lacking DE-SCs spontaneously induce epidermal genes *in vitro*. a Dental epithelial stem cell culture from CL tissues. **b** Left, representative brightfield images of DE-SC colonies and BrdU staining in Ctrl and *Med1* cKO. Bar = 10 μm. Right, quantification of colony size and BrdU positive cells/colony are shown as fold changes (cKO/Ctrl); in both comparisons p>0.01. **c** Biological processes associated to loss of *Med1* in DE-SCs as identified by Ingenuity Pathway Analysis (IPA) on microarray gene expression data. **d** Heatmap showing differential gene expressions of epidermal and hair related genes in *Med1* cKO vs Ctrl incisor tissues (CL and Sec *in vivo*) and cultured *Med1* cKO vs Ctrl DE-SCs (third lane) (n=3) for all samples and average values for each comparison are shown. **e** Upstream regulators responsible for biological process induced by loss of *Med1* in DE-SCs as identified by IPA on microarray data as used in (**c**). **f** Mechanistic network for TP53/63 pathways in induced in *Med1* cKO regulating epidermal fate driven AP-1 factors; upregulated genes are in orange and direct relationships are shown by solid lines. Reproducibility was confirmed by two independent cultures, and representative data are shown.

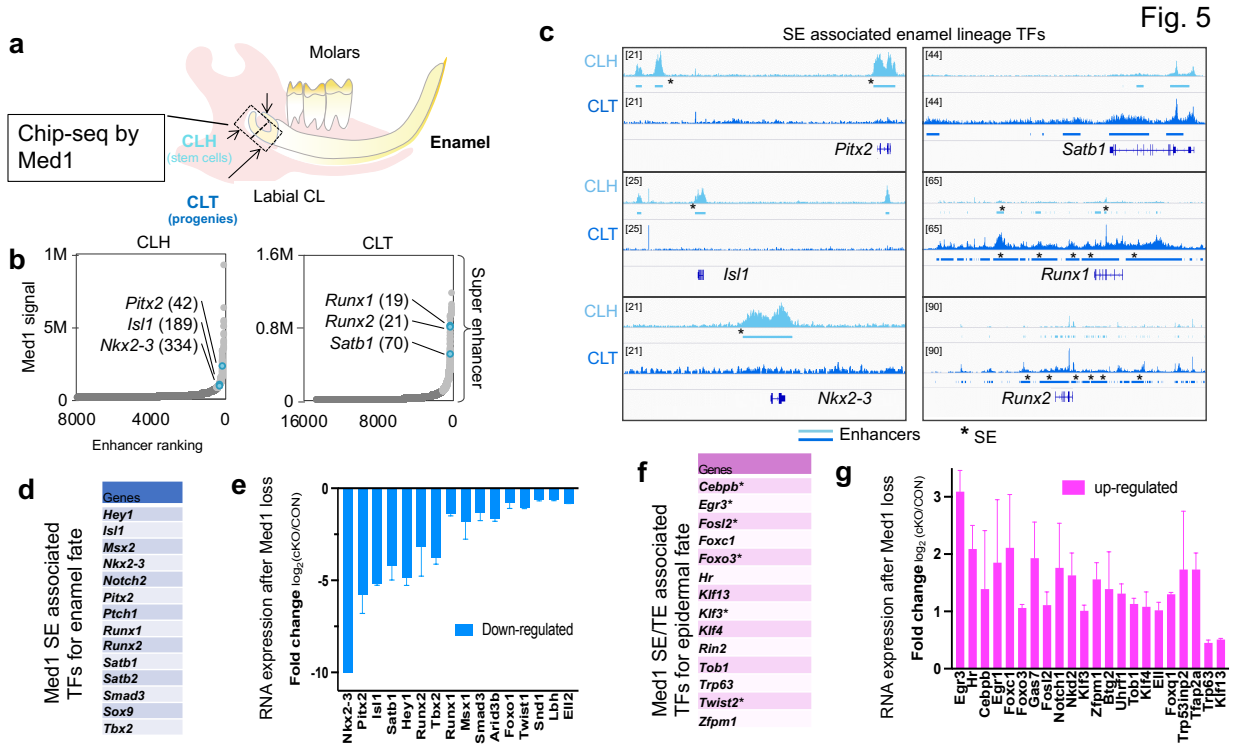

Fig. 5: Med1 directly controls enamel lineage controlling TFs by associating to their enhancers and promoter. a Schematic of isolation of CLH (stem cells) and CLT (progenies) from mouse mandible for Chip-seq using Med1 antibody. **b** Med1 bound enhancer distribution profiles to show SEs for critical TFs (blue circles) with ranking numbers in CLH and CLT. **c** Med1 Chip-seq profiles at CLH (light blue) and CLT (blue) to show the location of SEs (marked by bars with asterisks*) in *Pitx2, Nkx2-3, Isl, Satb1, Runx1/2* loci, in which average profiles of two independent Chip-seq experiments are shown. **d** Med1 SE identified a list of TFs. **e** Most of these TFs were down-regulated in *Med1 cKO* (CLT) in RNA-seq. **f** Another list of Med1 SE/TE associated TFs. **g** These TFs were upregulated in cKO (CLT) shown by RNA-seq, in which average and SD of fold changes (log_2FC) of two different litters of *Med1* cKO and control (3 mice each) with statistical significance $p<0.05$.

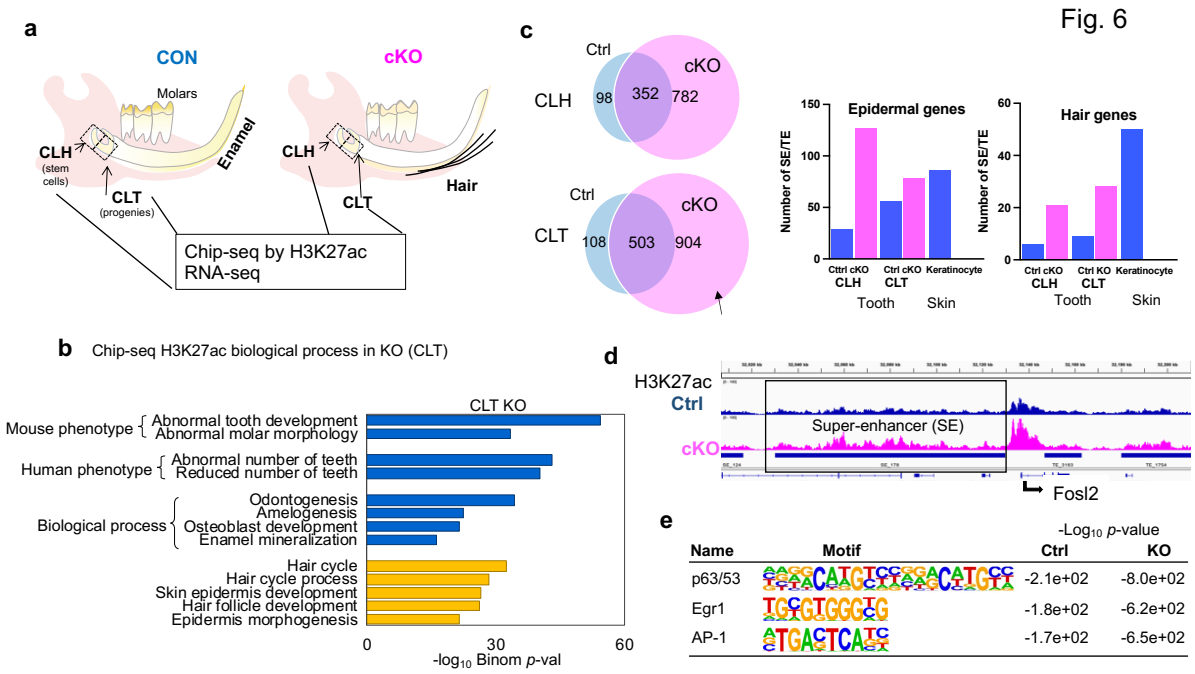

Fig. 6: Loss of *Med1* expands the H3K27ac super-enhancer landscape around epidermal and hair genes in CLH and CLT tissues. a Schematic of isolation of CLH (stem cells) and CLT (progenies) from *Med1* cKO and littermate CON mandible for parallel RNA-seq and Chip-seq for H3K27ac. **b** GREAT based GO analysis for differential H3K27ac peaks to elucidate biological process affected by *Med1* loss in CLT tissues. **c** Number of SEs in Ctrl (blue) and KO (pink) to show new SEs after loss of *Med1* in CLH and CLT tissues. Bar charts showing the increase in H3K27ac marked TE and SE after loss of *Med1* in CLH and CLT tissues around genomic loci for the gene-sets for epidermal and hair lineage genes, compared to ones for skin derived keratinocytes. **d** Chip-seq profiles for H3K27ac occupancy for *Fosl2* (Ap-1) gene, in which SEs is marked by underlying blue line. **e** Most enriched TF binding motifs found in SEs formed in *Med1* cKO and Ctrl in CLT tissues with statistical significance log(*p*-values). All the Chip-seq data are average of duplicates conducted in 2 different litters of *Med1* cKO and littermate control mice.

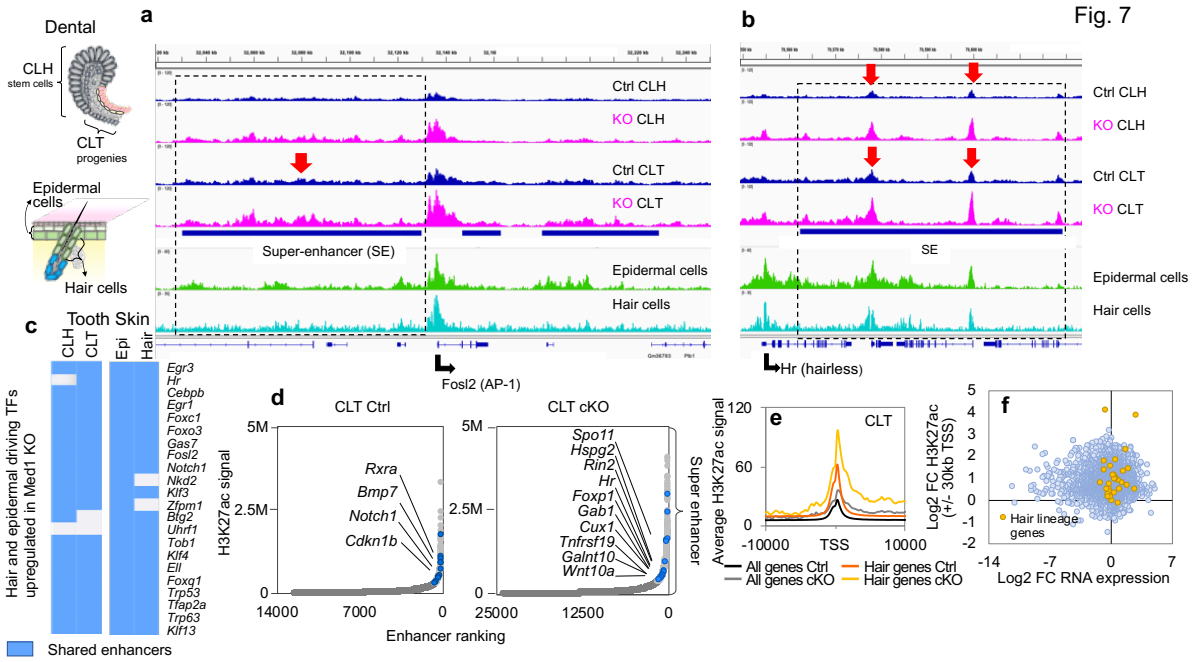

780

781

782 **Fig. 7: *Med1* cKO upgrades pre-existing enhancers to super-enhancer near**
783 **epidermal and hair lineage driving genes. a, b** Chip-seq H3K27ac profiles of dental stem
784 cells (CLH) and progenitor (CLT) for *Med1* cKO (pink) and CON (blue), compared to ones for
785 epidermal (green) and hair keratinocytes (light blue) from the skin in Fosl2 (**a**) and *Hr*
786 (hairless) loci (**b**). Pre-existing regular enhancers in Ctrl (red arrows) are transformed into
787 SE (blue bars) in *Med1* cKO at CLT. Schematic representations of cell sources are shown
788 (left). **c** Heatmap showing hair and epidermal lineage driving TFs, that are upregulated in
789 *Med1* cKO, share common enhancer profiles between dental epithelia (CLH and CLT)
790 and skin derived epidermal keratinocytes (Epi cells) and hair keratinocytes (hair cells). **d**
791 H3K27ac enhancer distribution profile, in which SEs associated with hair lineage driving
792 gene exclusively found in Ctrl or *Med1* cKO CLT tissues are noted by the gene names
793 (blue circles). **e** Average H3K27ac occupancy profiles around promoters of all genes vs
794 promoters of hair lineage driving factors in CLT Ctrl and CLT *Med1* cKO tissues. **f**
795 Correlation between gene expression and H3K27ac promoter occupancy (TSS +/-30 kb)
796 in *Med1* cKO vs Ctrl CLT tissues for the hair lineage driving gene set. FC, fold change.

797

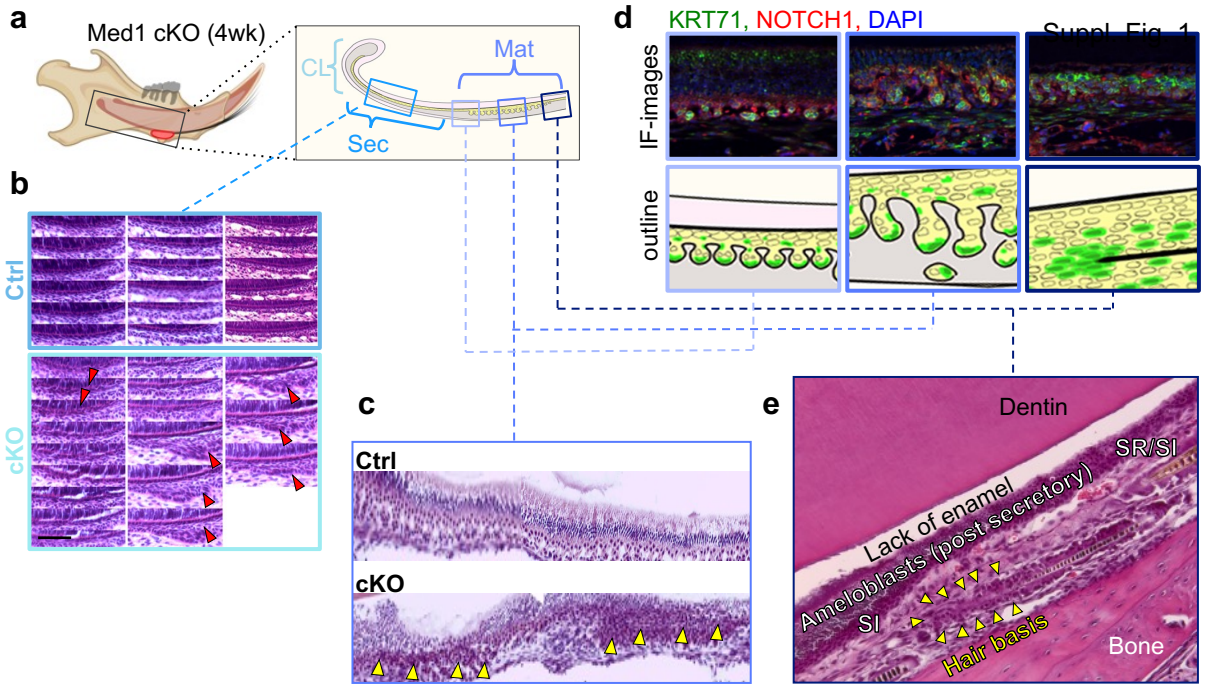

Suppl. Fig. 1: Histological and immuno-histological characterization of *Med1* cKO incisor tissue. a Diagram depicting the differentiation stages of mouse incisors including the location of the cervical loop (CL) and the secretory stage (Sec) and the maturation stage (Mat) of dental epithelia. Right, detailed representation of Sec and Mat. **b** Serial sectioning showing progression of abnormal stratum intermedium (SI) development with generation of atypical cell clusters (red triangles) in *Med1* cKO mice. **c** H&E staining to show abnormal expansion of papillary layer in cKO (yellow triangles). **d** Top, immuno-fluorescent visualization of Krt17 (green) and Notch1 (red) and DAPI counterstaining (blue) in SI/stellate reticulum (SR) derived papillary layers at different locations of the Mat stage. Bottom, diagram to show the locations of hair marker expression (green). **e** H&E-stained sections emphasizing the location of hair generating cell cluster found between dentin and bone in *Med1* cKO. SI, stratum intermedium, SR stellate reticulum.

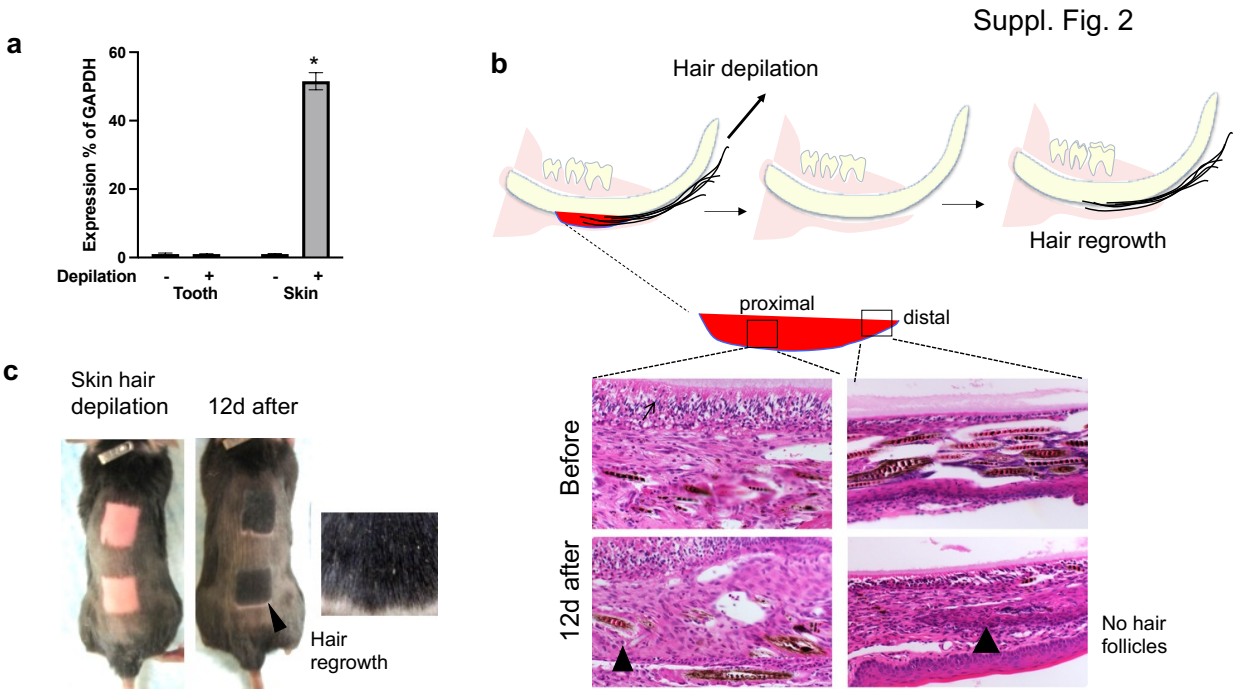

Suppl. Fig. 2: Effects of hair depilation on dental hair regeneration. a Hair marker *Krt31* mRNA expression in CL tissues of *Med1* cKO mice (tooth, left) and in normal skin tissue (skin right) before and 8 days after hair depilation. Representative data of average and SD of relative expression (% of GAPDH) and the statistical significance (n=3, * $p<0.05$). **b** Histological assessment of atypical hair generating cell clusters in *Med1* cKO incisors before and 12 days after hair depilation in proximal and distal region of the mandible corresponding to diagram. **c** Mouse skin shortly after hair depilation and 12 days post depilation, when hair is regrown (arrow) and enlarged image of hair.

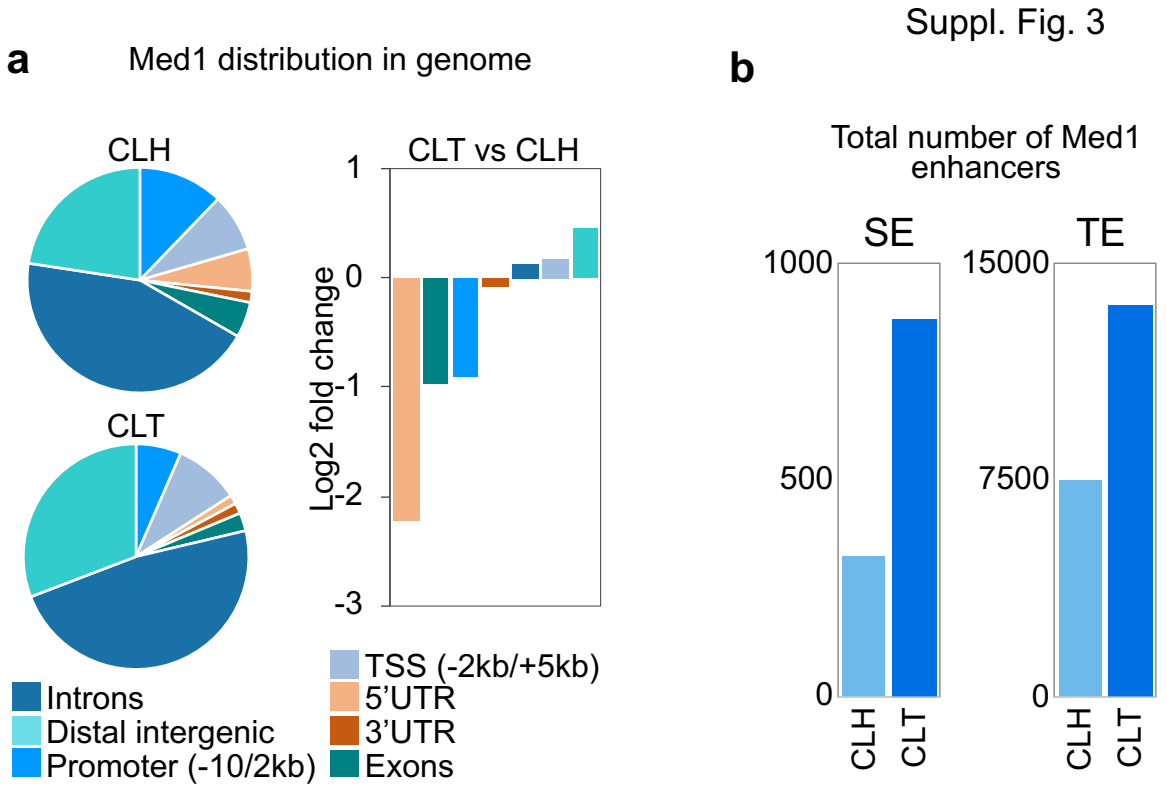

Suppl. Fig. 3: Med1 is distributed in different genomic regions in stem cells (CLH) and progenies (CLT).

a Relative distribution of Med1 binding at different genomic elements in CLH and CLT Ctrl tissues (left) and shift in Med1 binding at shown elements between CLT and CLH Ctrl tissues (right). **b** Total number of super enhancers (SE) and typical enhancers (TE) in CLH and CLT Ctrl tissues.

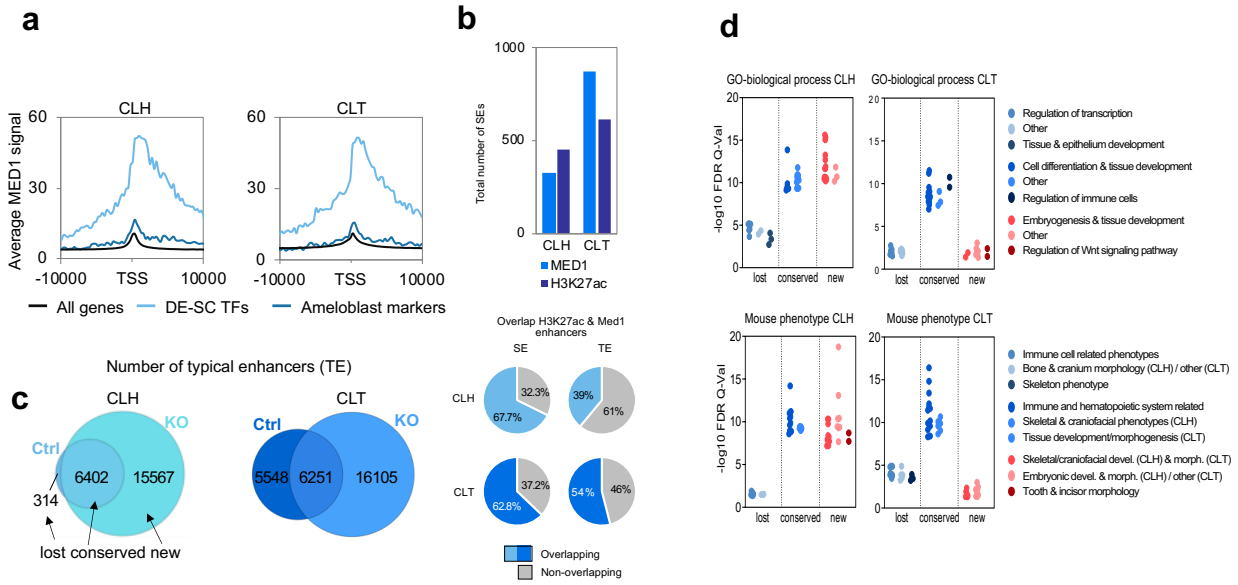

Suppl. Fig. 4: Med1 or H3K27ac occupancy dynamics in dental stem cells (CLH) and progenies (CLT)

a Average Med1 occupancy at promoters (TSS +/- 10kbp) for TFs driving enamel lineage, mature ameloblast markers and all other genes in CLH and CLT tissues. **b** H3K27ac or Med1 marked super enhancer (SE) and typical enhancer (TE) properties in CLH and CLT tissues. Total number of SEs in Ctrl CLH and CLT tissues (top) and overlapping Med1 and H3K27ac SEs and TEs (bottom). We observe that ~65% of H3K27ac SEs colocalize with Med1 SEs and when H3K27ac TEs are included in the overlap, a colocalization of 96-99% between Med1 SEs and H3K27ac SE/TE is obtained. Of note, we only find an overlap of 39% to 54% for TEs in CLH and CLT control tissues. **c** Total number of TEs, in which lost, conserved and new SEs in *Med1* cKO and Ctrl. **d** GREAT based GO-analysis on lost, conserved, and new H3K27ac SEs demonstrated in Fig 6c. Similar GO terms are summarized in common groups; terms defining GO-biological processes are shown on top and mouse phenotype related terms are shown on the bottom.

Suppl. Fig. 5

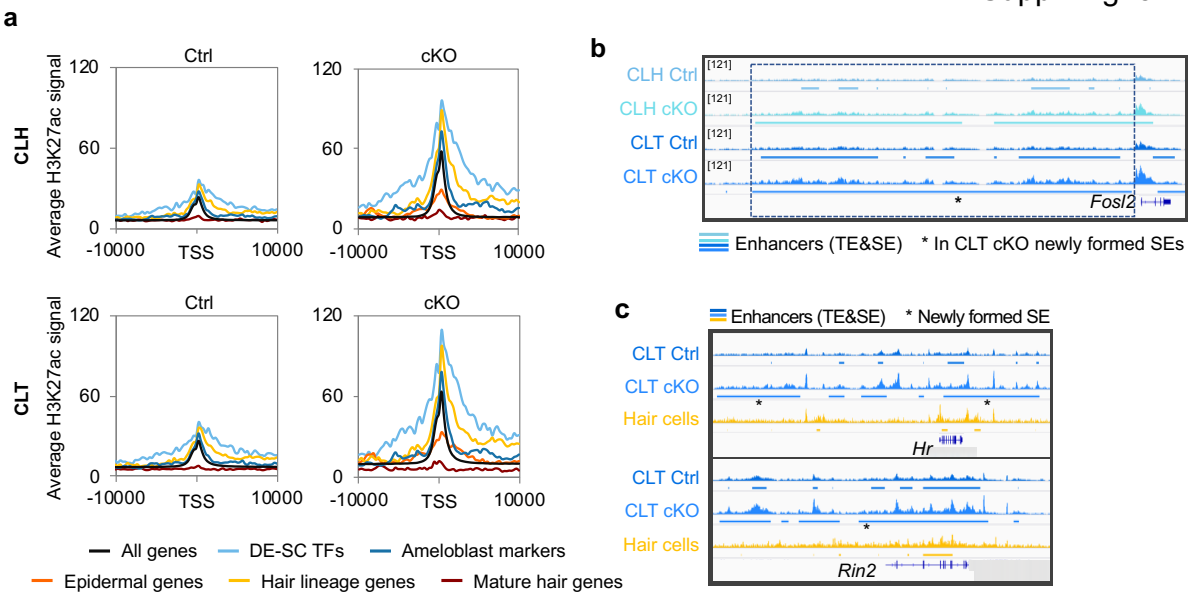

Suppl. Fig. 5: Genomic H3K27ac occupancy in promoters and enhancers and their changes in *Med1* cKO. a Average H3K27ac occupancy at promoters (TSS +/- 10kbp) for enamel lineage driven TFs, epidermal and hair lineage genes, ameloblast and mature hair markers in CLH and CLT tissues in *Med1* cKO (right panels) and Ctrl (left panels)**. b, c** H3K27ac occupancy around loci of epidermal *Fosl2* (**b**) and hair lineage driving TFs of *Hr* and *Rin2* (**c**) in Ctrl and *Med1* cKO CLT tissues as well as in skin derived hair keratinocytes. In *Med1* cKO CLT tissues, newly generated SEs are marked with asterisks (*).

Suppl. Fig. 6

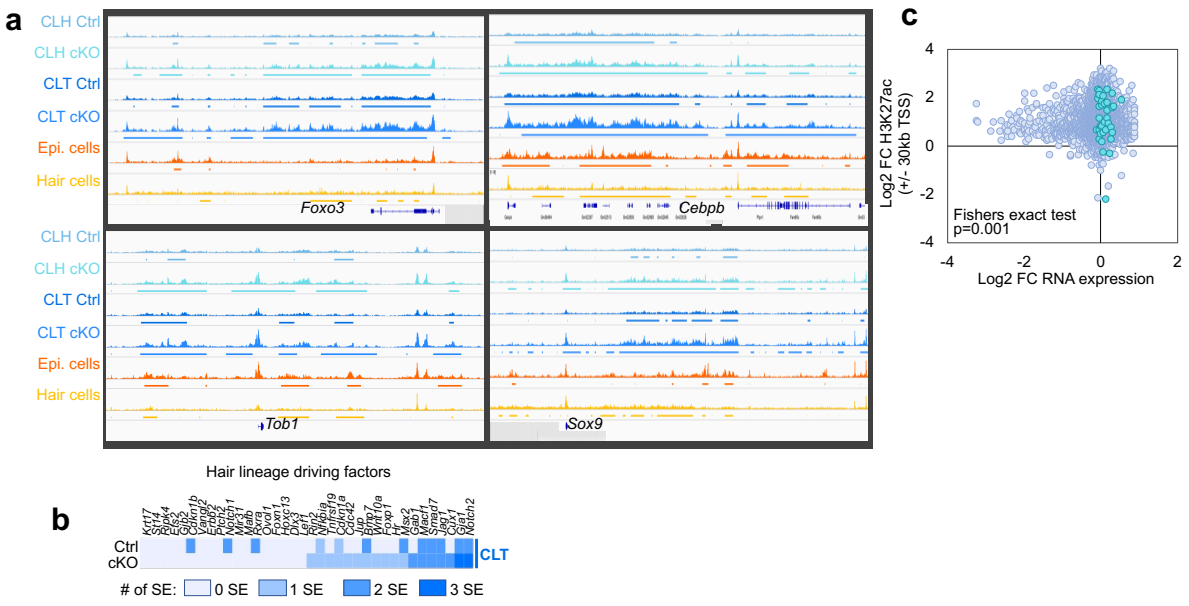

Suppl. Fig. 6: *Med1* deletion upgrades existing enhancers. a Chip-seq H3K27ac profiles around loci of epidermal driven TFs *Foxo3, Cebpb* and ossification inhibitory factors of *Tob1 and Sox9* that are upregulated in *Med1* cKO. Enhancers expand in size or heights in *Med1* cKO at CLT. Bars represent SE or TEs. Epi cells, epidermal cells. **b** H3K27ac SE dynamics for hair lineage driving genes between Ctrl and *Med1* null CLT tissues shown by the number of SEs for hair lineage genes, that are upregulated in *Med1* cKO at CLT. **c** Correlation between gene expression and H3K27ac promoter occupancy (TSS +/-30 kb) in *Med1* cKO vs Ctrl CLT tissues for the gene-set 'negative regulation of ossification' (blue circles) compared to all the other genes (pale blue).

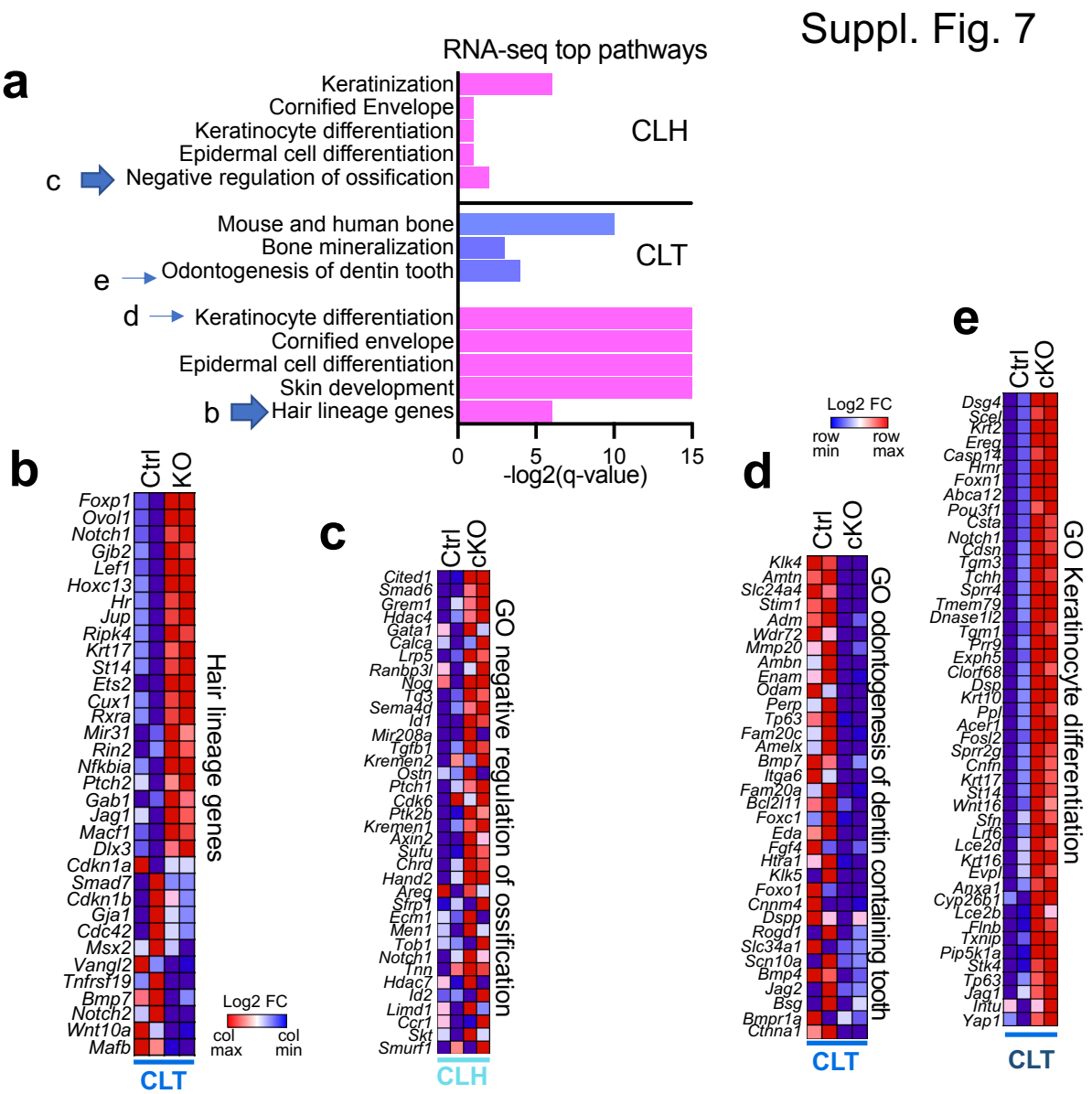

Suppl. Fig. 7: Differential mRNA expression at dental stem cells (CLH) and progenies (CLT) in *Med1* cKO (RNA-seq). a GO-based analysis on RNA-Seq expression data comparing *Med1* cKO vs Ctrl at CLH and CLT tissues at 4 wk (average of two litters). Annotations related to upregulated gene sets are shown in pink, and downregulated ones are shown in blue. Arrows show the potential causative pathways to cause cell fate conversion, that were further examined in Fig 7 and Suppl. Fig 6. Heatmaps for hair lineage genes (**b**), negative regulation of ossification (**c**), odontogenesis of dentin containing tooth including mature ameloblast markers (**d**), and increased keratinocyte differentiation markers (**e**).